

# Joint Transmitter and Receiver Design for Movable Antenna Enhanced Multicast Communications

Ying Gao, Qingqing Wu, *Senior Member, IEEE*, and Wen Chen, *Senior Member, IEEE*

**Abstract**—Movable antenna (MA) is an emerging technology that utilizes localized antenna movement to pursue better channel conditions for enhancing communication performance. In this paper, we study the MA-enhanced multicast transmission from a base station equipped with multiple MAs to multiple groups of single-MA users. Our goal is to maximize the minimum weighted signal-to-interference-plus-noise ratio (SINR) among all the users by jointly optimizing the position of each transmit/receive MA and the transmit beamforming. To tackle this challenging problem, we first consider the single-group scenario and propose an efficient algorithm based on the techniques of alternating optimization and successive convex approximation. Particularly, when optimizing transmit or receive MA positions, we construct a concave lower bound for the signal-to-noise ratio (SNR) of each user by applying only the second-order Taylor expansion, which is more effective than existing works utilizing two-step approximations. The proposed design is then extended to the general multi-group scenario. Simulation results demonstrate that significant performance gains in terms of achievable max-min SNR/SINR can be obtained by our proposed algorithm over benchmark schemes. Additionally, the proposed algorithm can notably reduce the required amount of transmit power or antennas for achieving a target level of max-min SNR/SINR performance compared to benchmark schemes.

**Index Terms**—Movable antenna, antenna position optimization, multi-group multicast, max-min fairness.

## I. INTRODUCTION

In recent decades, there has been a significant evolution in wireless communication technologies, transitioning from single-input-single-output (SISO) to multiple-input multiple-output (MIMO) [1]. By harnessing the independent or quasi-independent channel fading induced by the random superposition of multipath components, MIMO systems enable the simultaneous transmission of multiple data streams within the same time-frequency resource block, offering significant enhancements in spectral efficiency compared to single-antenna systems [2]–[4]. However, conventional MIMO systems typically employ fixed-position antennas (FPAs), and this static and discrete arrangement imposes constraints on their diversity and spatial multiplexing performance, leading to an incomplete exploitation of channel variations in the continuous spatial field. Therefore, despite the revolutionary impact of MIMO technologies on wireless communication, effectively leveraging spatial degrees of freedom (DoFs) in practical networks remains an ongoing challenge.

Recently, movable antenna (MA) [5]–[7], or fluid antenna [8], [9], has been considered as an innovative approach to

overcome the inherent limitations of traditional FPAs. Specifically, each MA is connected to the radio frequency chain via a flexible cable, and its position can be flexibly adjusted within a spatial region with the aid of mechanical controllers and drivers. Thus, unlike FPAs, which remain static and undergo random wireless channel variations, MAs can be strategically deployed at positions with better channel conditions to improve communication performance. In particular, MAs offer superior signal power enhancement, interference mitigation, flexible beamforming, and spatial multiplexing capabilities compared to FPAs [7]. Additionally, although the conventional antenna selection (AS) technique can also achieve spatial diversity gains, MAs are more cost-effective and efficient for two main reasons. Firstly, AS requires a large number of candidate antennas to select from, whereas MAs can fully utilize the spatial diversity in a given region with significantly fewer antennas. Secondly, antennas in AS systems are limited to discrete deployment at fixed locations in either a one-dimensional (1D) line or two-dimensional (2D) surface, while MAs can move freely within a three-dimensional (3D) space [7], [10], [11].

The appealing advantages of MAs have sparked significant interest in integrating them into various systems and optimizing their positions to achieve different design objectives. Initial studies in this field began with point-to-point single-user MA-enabled systems. For example, the authors of [5] proposed the mechanical MA architecture and a field-response for a SISO system consisting of a single-MA transmitter (Tx) and a single-MA receiver (Rx). They also analyzed the maximum signal-to-noise ratio (SNR) gain achieved by the single receive MA over its FPA counterpart under both deterministic and stochastic channels, assuming that the transmit MA is fixed at the reference point. Moreover, their analyses and simulations both demonstrated that the SNR gain of MA-enhanced systems over FPA-based systems is highly dependent on the number of channel paths and the size of the moving region for the receive MA. In [6], the authors investigated an MA-enabled point-to-point MIMO system and jointly optimized the transmit signals' covariance matrix and the positions of the MAs at the Tx/Rx to maximize the channel capacity. They proposed an alternating optimization (AO) algorithm to solve the considered problem suboptimally, wherein the optimization variables are iteratively and alternately optimized until convergence is reached. Numerical results showed that MA-enabled MIMO systems can achieve significantly higher capacity over conventional FPA-based MIMO systems with/without AS. Then, the works in [12] and [13] expanded upon the research conducted in [6] to address scenarios where only statistical channel state

The authors are with the Department of Electronic Engineering, Shanghai Jiao Tong University, Shanghai 201210, China (e-mail: yinggao@sjtu.edu.cn; qingqingwu@sjtu.edu.cn; whenchen@sjtu.edu.cn).

information (CSI) is available. Particularly, two simplified antenna movement modes, namely the linear movement mode and the planar movement mode, were proposed in [12]. The latter simplified mode was observed to demonstrate comparable performance to the general movement mode but with reduced computational and hardware complexities. Besides, for MA-enabled single-user systems, researchers investigated scenarios with one eavesdropper in [14], [15], and with multiple eavesdroppers in [16], [17]. Their simulation results all demonstrated the significant advantages of MA-enabled systems over FPA-based systems in enhancing system security performance. Unlike the aforementioned studies, which focused on narrow-band transmission in flat fading channels, the research in [18] utilized MAs to enhance the wideband communication between a Tx and an Rx.

Meanwhile, there have been some studies on more general MA-assisted multiuser systems. In [19], the authors studied the MA-enhanced uplink transmission from multiple single-MA users to a base station (BS) equipped with an FPA array. They proposed two suboptimal algorithms to minimize the total transmit power at the users while satisfying each user's minimum achievable rate requirement, determining the positions of MAs using the gradient descent method in an iterative manner. Simulation results demonstrated a notable reduction in the total transmit power of MA-enhanced systems compared to their FPA counterparts. Following [19], the authors of [20] also investigated the transmit power minimization problem for an MA-aided multiuser uplink communication system, but the difference lies in that the BS is equipped with a linear MA array and the users are all single-FPA devices. Unlike [19] which exploits the original definition-based method, [20] developed a projected gradient descent-based algorithm with low complexity. If the receive MAs at the BS can move in a 2D region, then the system model studied in [20] is consistent to the one investigated in [21]. To enhance user fairness, the authors of [21] proposed a two-loop iterative algorithm utilizing the particle swarm optimization method.

Apart from the above research focusing on uplink scenarios, the works in [22]–[30] explored MA-enabled multiuser downlink communication systems. Notably, in [22], the authors investigated the amalgamation of MA and reconfigurable intelligent surface. In [29], a hybrid beamforming scheme with a sub-connected structure was proposed. Simulation results showed that when the moving regions are sufficiently large, the proposed scheme with sub-connected MA arrays even outperforms the fully-connected FPA array in achievable sum rate. In [30], the authors modeled the motion of MAs as discrete movements and studied the transmit power minimization subject to the minimum required signal-to-interference-plus-noise ratio (SINR) of each user. Moreover, the authors of [31] and [32] respectively studied MA-enabled symbiotic radio communications and MA-enabled full-duplex communications. In addition to all the above works that are limited to single-cell scenarios, the authors of [33] investigated an MA-aided multi-cell multiple-input single-output (MISO) interference channel. Their numerical results showed MAs' benefits in enhancing inter-cell frequency reuse capability. On the other hand, since the knowledge of CSI across the entire

moving region is crucial for optimizing the positions of MAs to improve system performance, some research efforts have been devoted to studying the channel estimation for MA-enabled wireless communications (see, e.g., [34]–[36]).

Although several works have demonstrated the benefits of employing MAs in various systems, their potential for multicast communications, which are highly efficient for common information broadcasting in practice (e.g., live video streaming and live games), remains unexplored. In multicast communication systems, attaining (weighted) max-min fairness (MMF) among users is a pivotal consideration. With the spatial diversity and interference mitigation gains offered by MAs, MA-enabled multicast communication systems are expected to significantly outperform their FPA counterparts in terms of MMF. Furthermore, if we consider a MISO setup where the BS is equipped with multiple MAs and each user is equipped with a single MA, it is intriguing to see whether employing transmit MAs or receive MAs yields better performance, assuming that the transmit region and each receive region have identical sizes. The comparison results may provide useful engineering insights into the practical deployment of MAs. For the case employing receive MAs, it is feasible for all users to achieve their individual maximum SNR/SINR simultaneously through strategic positioning of receive MAs. In contrast, for the case employing transmit MAs, users are consistently in competition for resources, and there is always a non-trivial trade-off among users' SNR/SINR. More specifically, the positioning of each transmit MA needs to weigh the trade-offs among the channel conditions of all users, and improving the SNR/SINR of one user often comes at the cost of decreasing the SNR/SINR of others. Thus, receive MAs may provide a more significant performance enhancement in achievable max-min SNR/SINR than transmit MAs, even when their number is slightly less than that of transmit MAs, let alone when their number exceeds that of transmit MAs.

Motivated by the above discussions, this paper investigates an MA-enabled multicast MISO communication system which is composed of a BS with  $M$  transmit MAs and  $N$  groups with a total of  $K$  single-MA users overall, as shown in Fig. 1. The main contributions of this paper are summarized as follows:

- To the best of the authors' knowledge, this is the first work in the literature to study MA-enhanced multicast transmission. We formulate a minimum weighted SINR maximization problem that jointly optimizes the positions of transmit/receive MAs and the transmit beamforming, under the constraints of maximum transmit power at the BS, finite moving region for each MA, and minimum inter-MA distance.
- To handle the non-convex and challenging optimization problem, we first consider a simplified scenario with only one group and propose an efficient AO algorithm, which will serve as a building block for the general multi-group scenario. Specifically, the transmit precoder, the position of each transmit MA, and the positions of all the receive MAs are iteratively optimized based on the successive convex approximation (SCA) technique. In particular, when optimizing transmit or receive MA positions, we construct a concave lower bound for each user's SNR by

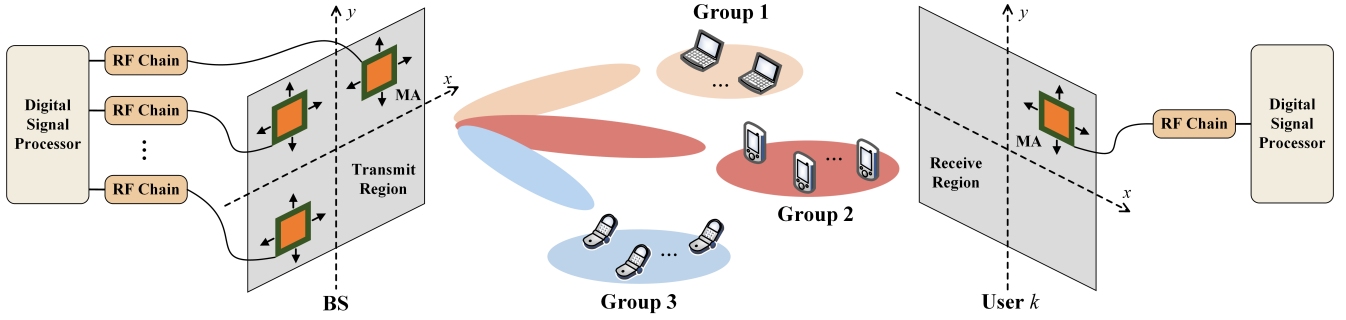


Fig. 1. Illustration of an MA-enhanced multi-group multicast MISO communication system.

applying only the second-order Taylor expansion. This distinguishes our proposed algorithm from the method introduced in [6], which requires applying the first-order Taylor expansion before the second-order Taylor expansion. Subsequently, we extend the proposed algorithm to the general case with multiple groups by introducing slack variables.

- Numerical results demonstrate that: 1) our proposed algorithm is more effective than the method presented in [6]; 2) the proposed algorithm performs much better than the benchmark schemes (especially its counterpart with FPAs at both the BS and the users) in terms of achievable max-min SNR/SINR under various setups; 3) there is a notable reduction in the required amount of transmit power or antennas to achieve a target level of max-min SNR/SINR performance with the proposed algorithm compared to benchmark schemes; 4) under the assumption that the transmit region and each receive region have identical sizes, employing only receive MAs results in higher max-min SNR/SINR than employing only transmit MAs when  $M \leq K$ , and this remains true even when  $M$  is slightly larger than  $K$ .

The rest of this paper is organized as follows. Section II introduces the system model and formulates the minimum SINR maximization problem for an MA-enabled multi-group multicast communication system. An efficient algorithm is proposed in Section III for addressing the simplified scenario with only one group, which is subsequently extended to handle the general multi-group scenario in Section IV. We evaluate the performance of our proposed algorithm via simulations in Section V. Finally, Section VI concludes the paper.

*Notations:*  $\mathbb{C}$  denotes the complex space.  $\mathbb{C}^{M \times N}$  represents the space of  $M \times N$  complex-valued matrices. For a complex-valued number  $x$ ,  $|x|$ ,  $\text{Re}\{\cdot\}$ , and  $\arg(x)$  denote its modulus, real part, and phase argument, respectively. For a complex-valued vector  $\mathbf{a}$ ,  $\|\mathbf{a}\|$  and  $[\mathbf{a}]_i$  denote its Euclidean norm and  $i$ -th element, respectively. For a matrix  $\mathbf{A}$  of arbitrary size,  $\|\mathbf{A}\|_2$ ,  $\|\mathbf{A}\|_F$ , and  $[\mathbf{A}]_{i,j}$  represent its spectral norm, Frobenius norm, and  $(i, j)$ -th element, respectively. For two square matrices  $\mathbf{S}_1$  and  $\mathbf{S}_2$ ,  $\mathbf{S}_1 \succeq \mathbf{S}_2$  indicates that  $\mathbf{S}_1 - \mathbf{S}_2$  is positive semidefinite. For a set  $\mathcal{X}$ ,  $|\mathcal{X}|$  denotes its cardinality.  $\mathbf{I}$  is an identity matrix whose dimension is determined by the context. The conjugate transpose operator is denoted by  $(\cdot)^H$ , while the expectation operator is represented by  $\mathbb{E}(\cdot)$ .  $\text{diag}(\cdot)$

denotes the diagonalization operation.  $\mathcal{CN}(\mathbf{x}, \mathbf{\Sigma})$  represents a complex Gaussian distribution with a mean vector  $\mathbf{x}$  and co-variance matrix  $\mathbf{\Sigma}$ .  $j \triangleq \sqrt{-1}$  refers to the imaginary unit.

## II. SYSTEM MODEL AND PROBLEM FORMULATION

### A. System Model

As shown in Fig. 1, we consider an MA-enabled multi-group multicast communication system, where a BS equipped with  $M$  transmit MAs serves  $K$  single-MA users grouped into  $N$  ( $1 \leq N \leq K$ ) multicast groups. The set of transmit MAs and users are denoted by  $\mathcal{M}$  and  $\mathcal{K}$ , respectively, with  $|\mathcal{M}| = M$  and  $|\mathcal{K}| = K$ . Let  $\mathcal{G}_n$  denote the set of users in group  $n$ ,  $n \in \mathcal{N} \triangleq \{1, \dots, N\}$ . Each user belongs to only one group, hence  $\mathcal{G}_n \cap \mathcal{G}_q = \emptyset, \forall n, q \in \mathcal{N}$  and  $\bigcup_{n=1}^N \mathcal{G}_n = \mathcal{K}$ . In addition, the transmit and receive MAs are connected to RF chains via flexible cables, enabling them to move freely within local regions [5], [16]. Let  $\mathcal{C}^t$  denote the given 2D moving region for the  $M$  transmit MAs. The 2D moving region for the single MA at user  $k$  is denoted by  $\mathcal{C}_k^r$ . Without loss of generality, we assume that both  $\mathcal{C}^t$  and  $\mathcal{C}_k^r$  are square regions of size  $A \times A$ . The positions of the  $m$ -th transmit MA at the BS and the single receive MA at the  $k$ -th user are represented by  $\mathbf{t}_m = [x_m^t, y_m^t]^T \in \mathcal{C}^t$  and  $\mathbf{r}_k = [x_k^r, y_k^r]^T \in \mathcal{C}_k^r$ , respectively. The reference points in the regions  $\mathcal{C}^t$  and  $\mathcal{C}_k^r$  are denoted by  $\mathbf{o}^t = [0, 0]^T$  and  $\mathbf{o}_k^r = [0, 0]^T$ , respectively.

The assumption is made that the sizes of the antenna moving regions are considerably smaller than the signal propagation distance, ensuring that the far-field condition is satisfied between the BS and the users. In this case, for each channel path component, altering the MA positions has no impact on the angle of departure (AoD), the angle of arrival (AoA), and the amplitude of the complex coefficient, but solely influences the phase of the complex coefficient. Denote the total number of transmit and receive channel paths from the BS to user  $k$  as  $L_k^t$  and  $L_k^r$ , respectively. The elevation and azimuth AoDs of the  $i$ -th transmit path for user  $k$  are denoted by  $\theta_{k,i}^t \in [-\frac{\pi}{2}, \frac{\pi}{2}]$  and  $\phi_{k,i}^t \in [-\frac{\pi}{2}, \frac{\pi}{2}]$ , respectively. The elevation and azimuth AoAs of the  $j$ -th receive path for user  $k$  are denoted by  $\theta_{k,j}^r \in [-\frac{\pi}{2}, \frac{\pi}{2}]$  and  $\phi_{k,j}^r \in [-\frac{\pi}{2}, \frac{\pi}{2}]$ , respectively. Then, for user  $k$ , the propagation distance difference of the  $i$ -th transmit path between positions  $\mathbf{t}_m$  and  $\mathbf{o}^t$  is given by  $\mathbf{t}_m^T [\cos \theta_{k,i}^t, \sin \phi_{k,i}^t, \sin \theta_{k,i}^t]^T \triangleq \mathbf{t}_m^T \mathbf{a}_{k,i}^t$  [5]. Accordingly, the phase difference of the  $m$ -th transmit path between positions

$\mathbf{t}_m$  and  $\mathbf{o}^t$  is obtained as  $\frac{2\pi}{\lambda} \mathbf{t}_m^T \mathbf{a}_{k,i}^t$ , where  $\lambda$  denotes the carrier wavelength. To account for the phase differences in all  $L_k^t$  transmit paths from the BS to user  $k$ , the field-response vector of the  $m$ -th MA at the BS is written as

$$\mathbf{g}_k(\mathbf{t}_m) = \left[ e^{j\frac{2\pi}{\lambda} \mathbf{t}_m^T \mathbf{a}_{k,1}^t}, e^{j\frac{2\pi}{\lambda} \mathbf{t}_m^T \mathbf{a}_{k,2}^t}, \dots, e^{j\frac{2\pi}{\lambda} \mathbf{t}_m^T \mathbf{a}_{k,L_k^t}^t} \right]^T. \quad (1)$$

We stack  $\{\mathbf{g}_k(\mathbf{t}_m)\}$  into a matrix to obtain the field-response matrix at the BS, represented as

$$\mathbf{G}_k(\mathbf{t}) = [\mathbf{g}_k(\mathbf{t}_1), \mathbf{g}_k(\mathbf{t}_2), \dots, \mathbf{g}_k(\mathbf{t}_M)] \in \mathbb{C}^{L_k^t \times M}, \quad (2)$$

where  $\mathbf{t} \triangleq \{\mathbf{t}_m\}$ . Similar to (1), the field-response vector of the receive MA at the  $k$ -th user is given by

$$\mathbf{f}_k(\mathbf{r}_k) = \left[ e^{j\frac{2\pi}{\lambda} \mathbf{r}_k^T \mathbf{a}_{k,1}^r}, e^{j\frac{2\pi}{\lambda} \mathbf{r}_k^T \mathbf{a}_{k,2}^r}, \dots, e^{j\frac{2\pi}{\lambda} \mathbf{r}_k^T \mathbf{a}_{k,L_k^r}^r} \right]^T, \quad (3)$$

where  $\mathbf{a}_{k,j}^r \triangleq [\cos \theta_{k,j}^r, \sin \phi_{k,j}^r, \sin \theta_{k,j}^r]^T$ . Furthermore, let  $\Sigma_k \in \mathbb{C}^{L_k^r \times L_k^t}$  represent the path-response matrix, which characterizes the responses between all the transmit and receive channel paths from  $\mathbf{o}^t$  to  $\mathbf{o}_k^r$ . Then, the channel vector between the BS and the  $k$ -th user can be expressed as

$$\mathbf{h}_k(\mathbf{t}, \mathbf{r}_k)^H = \mathbf{f}_k(\mathbf{r}_k)^H \Sigma_k \mathbf{G}_k(\mathbf{t}) \in \mathbb{C}^{1 \times M}. \quad (4)$$

For multi-group multicast systems, users within the same group share the same message, while the messages required by different groups are independent of each other. At the BS, we consider a linear transmit precoding with  $\mathbf{w}_n$  denoting the beamforming vector for group  $n$ . The transmitted signal from the BS is then given by  $\mathbf{x} = \sum_{n=1}^N \mathbf{w}_n s_n$ , where  $s_n$  denotes the data symbol for group  $n$  and  $\{s_n\}$  are independent over  $n$ , satisfying  $\mathbb{E}(|s_n|^2) = 1, \forall n \in \mathcal{N}$ . The corresponding received signal at user  $k \in \mathcal{G}_n$  can be written as

$$y_k = \mathbf{h}_k(\mathbf{t}, \mathbf{r}_k)^H \mathbf{w}_n s_n + \sum_{q=1, q \neq n}^N \mathbf{h}_k(\mathbf{t}, \mathbf{r}_k)^H \mathbf{w}_q s_q + z_k, \quad (5)$$

where  $z_k \sim \mathcal{CN}(0, \sigma_k^2)$  denotes the additive white Gaussian noise with variance  $\sigma_k^2$  at user  $k$ . As a result, the SINR of user  $k \in \mathcal{G}_n$  is given by

$$\text{SINR}_k = \frac{|\mathbf{h}_k(\mathbf{t}, \mathbf{r}_k)^H \mathbf{w}_n|^2}{\sum_{q=1, q \neq n}^N |\mathbf{h}_k(\mathbf{t}, \mathbf{r}_k)^H \mathbf{w}_q|^2 + \sigma_k^2}. \quad (6)$$

### B. Problem Formulation

In this paper, we aim to maximize the minimum weighted SINR among all the users by jointly optimizing the transmit precoders  $\{\mathbf{w}_n\}$ , the transmit MA positions  $\{\mathbf{t}_m\}$ , and the receive MA positions  $\{\mathbf{r}_k\}$ . The problem of interest can be formulated as

$$(P1): \max_{\eta, \{\mathbf{w}_n\}, \{\mathbf{t}_m\}, \{\mathbf{r}_k\}} \eta \quad (7a)$$

$$\text{s.t.} \quad \frac{1}{\gamma_k} \frac{|\mathbf{h}_k(\mathbf{t}, \mathbf{r}_k)^H \mathbf{w}_n|^2}{\sum_{q=1, q \neq n}^N |\mathbf{h}_k(\mathbf{t}, \mathbf{r}_k)^H \mathbf{w}_q|^2 + \sigma_k^2} \geq \eta, \quad \forall k \in \mathcal{G}_n, n \in \mathcal{N}, \quad (7b)$$

$$\sum_{n=1}^N \|\mathbf{w}_n\|^2 \leq P_{\max}, \quad (7c)$$

$$\mathbf{t}_m \in \mathcal{C}^t, \forall m \in \mathcal{M}, \quad (7d)$$

$$\|\mathbf{t}_m - \mathbf{t}_p\| \geq D, \forall m, p \in \mathcal{M}, m \neq p, \quad (7e)$$

$$\mathbf{r}_k \in \mathcal{C}_k^r, \forall k \in \mathcal{K}, \quad (7f)$$

where  $\gamma_k$  in (7b) is the weighting factor controlling the service priority of user  $k$ ,  $P_{\max} > 0$  in (7c) represents the maximum instantaneous transmit power of the BS, and (7e) ensures that the distance between each pair of transmit MAs is no smaller than  $D > 0$  to avoid the coupling effect between them. We note that  $\{\mathbf{w}_n\}, \{\mathbf{t}_m\}, \{\mathbf{r}_k\}$  are intricately coupled in constraint (7b). This, along with the non-convex minimum distance constraint (7e), renders (P1) to be a non-convex optimization problem that presents challenges in seeking an optimal solution. To tackle this issue, we first address the single-group scenario, laying the groundwork for handling the more complex multi-group scenario. Specifically, in the next section, we propose an efficient algorithm to solve (P1) for the single-group case, which is then extended to the multi-group case in Section IV.

### III. SINGLE-GROUP SCENARIO

In this section, we focus on the single-group scenario, i.e.,  $N = 1$ , and omit the group index  $n$  for brevity. In this case, due to the absence of inter-group interference, (P1) can be simplified as

$$(P2): \max_{\eta, \mathbf{w}, \{\mathbf{t}_m\}, \{\mathbf{r}_k\}} \eta \quad (8a)$$

$$\text{s.t.} \quad \frac{1}{\gamma_k} \frac{|\mathbf{h}_k(\mathbf{t}, \mathbf{r}_k)^H \mathbf{w}|^2}{\sigma_k^2} \geq \eta, \forall k \in \mathcal{K}, \quad (8b)$$

$$\|\mathbf{w}\|^2 \leq P_{\max}, \quad (8c)$$

$$(7d) - (7f). \quad (8d)$$

While (P2) is much simplified compared to (P1), it remains a non-convex optimization problem because the left-hand-side (LHS) of (8b) is not jointly concave with respect to (w.r.t.)  $\{\mathbf{w}, \{\mathbf{t}_m\}, \{\mathbf{r}_k\}\}$ , and the non-convex constraint (7e) still exists. In the following, we explore an efficient AO-based method to address (P2) featuring coupled optimization variables.

#### A. Optimizing $\mathbf{w}$ for Given $\{\{\mathbf{t}_m\}, \{\mathbf{r}_k\}\}$

When all the MA positions are given, (P2) reduces to the classical max-min fair beamforming problem in single-group multicast systems, as follows:

$$\max_{\eta, \mathbf{w}} \eta \quad (9a)$$

$$\text{s.t.} \quad \mathbf{w}^H \mathbf{H}_k(\mathbf{t}, \mathbf{r}_k) \mathbf{w} \geq \eta \gamma_k \sigma_k^2, \forall k \in \mathcal{K}, \quad (9b)$$

$$(8c), \quad (9c)$$

where  $\mathbf{H}_k(\mathbf{t}, \mathbf{r}_k) \triangleq \mathbf{h}_k(\mathbf{t}, \mathbf{r}_k) \mathbf{h}_k(\mathbf{t}, \mathbf{r}_k)^H$ . Although problem (9) is non-convex due to the convexity of  $\mathbf{w}^H \mathbf{H}_k(\mathbf{t}, \mathbf{r}_k) \mathbf{w}$  in (9b), it can be efficiently solved by using the SCA technique. To elaborate, by replacing  $\mathbf{w}^H \mathbf{H}_k(\mathbf{t}, \mathbf{r}_k) \mathbf{w}$  with its global

under-estimator based on the first-order Taylor expansion, problem (9) can be approximated as

$$\max_{\eta, \mathbf{w}} \eta \quad (10a)$$

$$\text{s.t. } 2\text{Re} \left\{ (\mathbf{w}^\ell)^H \mathbf{H}_k(\mathbf{t}, \mathbf{r}_k) \mathbf{w} \right\} - (\mathbf{w}^\ell)^H \mathbf{H}_k(\mathbf{t}, \mathbf{r}_k) \mathbf{w}^\ell \geq \eta \gamma_k \sigma_k^2, \quad \forall k \in \mathcal{K}, \quad (10b)$$

$$(8c), \quad (10c)$$

where  $\mathbf{w}^\ell$  denotes the given local point in the  $\ell$ -th iteration. Problem (10) is a convex quadratically constrained program (QCP) that can be optimally solved utilizing existing solvers like CVX [37].

### B. Optimizing $\mathbf{t}_m$ for Given $\{\mathbf{w}, \{\mathbf{t}_p\}_{p \in \mathcal{M} \setminus \{m\}}, \{\mathbf{r}_k\}\}$

For any given  $\{\mathbf{w}, \{\mathbf{t}_p\}_{p \in \mathcal{M} \setminus \{m\}}, \{\mathbf{r}_k\}\}$ , the subproblem of (P2) for optimizing  $\mathbf{t}_m$  is given by

$$\max_{\eta, \mathbf{t}_m} \eta \quad (11a)$$

$$\text{s.t. } |\mathbf{h}_k(\mathbf{t}, \mathbf{r}_k)^H \mathbf{w}|^2 \geq \eta \gamma_k \sigma_k^2, \quad \forall k \in \mathcal{K}, \quad (11b)$$

$$\mathbf{t}_m \in \mathcal{C}^t, \quad (11c)$$

$$\|\mathbf{t}_m - \mathbf{t}_p\| \geq D, \quad \forall p \in \mathcal{M}, p \neq m. \quad (11d)$$

We notice that the optimization variable  $\mathbf{t}_m$  is not exposed in the current form of constraint (11b). Recall that  $\mathbf{h}_k(\mathbf{t}, \mathbf{r}_k)^H = \mathbf{f}_k(\mathbf{r}_k)^H \mathbf{\Sigma}_k \mathbf{G}_k(\mathbf{t})$ . To facilitate the solution design, we define  $\mathbf{b}_k^H \triangleq \mathbf{f}_k(\mathbf{r}_k)^H \mathbf{\Sigma}_k \in \mathbb{C}^{1 \times L_k^t}$  and expand the LHS of constraint (11b) in (12), as shown at the bottom of this page. In (12),  $w_m$  is the  $m$ -th element of  $\mathbf{w}$ ,  $\Lambda_{k,m} \triangleq \sum_{p=1, p \neq m}^M \mathbf{b}_k^H \mathbf{g}_k(\mathbf{t}_p) w_p$ ,  $\mathbf{B}_k \triangleq \mathbf{b}_k \mathbf{b}_k^H$ ,  $\beta_{i,j,k}(\mathbf{t}_m) \triangleq \frac{2\pi}{\lambda} \mathbf{t}_m^T (-\mathbf{a}_{k,i}^t + \mathbf{a}_{k,j}^t) + \arg([\mathbf{B}_k]_{i,j})$ , and  $\iota_{k,i}(\mathbf{t}_m) \triangleq \frac{2\pi}{\lambda} \mathbf{t}_m^T \mathbf{a}_{k,i}^t + \arg(w_m) - \arg(\Lambda_{k,m}) - \arg([\mathbf{b}_k]_i)$ . With (12), constraint (11b) can be recast as

$$u_k(\mathbf{t}_m) \geq \eta \gamma_k \sigma_k^2, \quad \forall k \in \mathcal{K}. \quad (13)$$

However,  $u_k(\mathbf{t}_m)$  is neither concave nor convex w.r.t.  $\mathbf{t}_m$ , making constraint (13) still non-convex and also preventing us from constructing a global lower bound for  $u_k(\mathbf{t}_m)$  based on its first-order Taylor expansion. To handle (13), we construct a concave lower-bound surrogate function for  $u_k(\mathbf{t}_m)$  by applying the second-order Taylor expansion. Specifically, with a positive real number  $\psi_{k,m}$  such that  $\psi_{k,m} \mathbf{I} \succeq \nabla^2 u_k(\mathbf{t}_m)$ , the following inequality holds:

$$\begin{aligned} u_k(\mathbf{t}_m) &\geq u_k(\mathbf{t}_m^\ell) + \nabla u_k(\mathbf{t}_m^\ell)^T (\mathbf{t}_m - \mathbf{t}_m^\ell) \\ &\quad - \frac{\psi_{k,m}}{2} (\mathbf{t}_m - \mathbf{t}_m^\ell)^T (\mathbf{t}_m - \mathbf{t}_m^\ell) \\ &\triangleq u_k^{\text{lb},\ell}(\mathbf{t}_m), \end{aligned} \quad (14)$$

which is obtained by modifying [38, Lemma 12]. In (14),  $\mathbf{t}_m^\ell$  is the given local point in the  $\ell$ -th iteration and  $\nabla u_k(\mathbf{t}_m^\ell)^T = \left[ \frac{\partial u_k(\mathbf{t}_m)}{\partial x_m^t} \Big|_{\mathbf{t}_m = \mathbf{t}_m^\ell}, \frac{\partial u_k(\mathbf{t}_m)}{\partial y_m^t} \Big|_{\mathbf{t}_m = \mathbf{t}_m^\ell} \right]$  with the expressions of  $\frac{\partial u_k(\mathbf{t}_m)}{\partial x_m^t} \Big|_{\mathbf{t}_m = \mathbf{t}_m^\ell}$  and  $\frac{\partial u_k(\mathbf{t}_m)}{\partial y_m^t} \Big|_{\mathbf{t}_m = \mathbf{t}_m^\ell}$  given in (15) at the bottom of the following page. Next, we show how to find a  $\psi_{k,m}$ . First, we derive the Hessian matrix of  $u_k(\mathbf{t}_m)$ ,  $\nabla^2 u_k(\mathbf{t}_m)$ , as

$$\nabla^2 u_k(\mathbf{t}_m) = \begin{bmatrix} \frac{\partial u_k(\mathbf{t}_m)}{\partial x_m^t} & \frac{\partial u_k(\mathbf{t}_m)}{\partial x_m^t \partial y_m^t} \\ \frac{\partial u_k(\mathbf{t}_m)}{\partial y_m^t} & \frac{\partial u_k(\mathbf{t}_m)}{\partial y_m^t \partial y_m^t} \end{bmatrix}, \quad (16)$$

where the expressions of the matrix's elements are provided in (17) at the bottom of the subsequent page. Second, we have

$$\begin{aligned} \|\nabla^2 u_k(\mathbf{t}_m)\|_2 &\leq \|\nabla^2 u_k(\mathbf{t}_m)\|_F \\ &= \left[ \left( \frac{\partial u_k(\mathbf{t}_m)}{\partial x_m^t} \right)^2 + \left( \frac{\partial u_k(\mathbf{t}_m)}{\partial x_m^t \partial y_m^t} \right)^2 + \left( \frac{\partial u_k(\mathbf{t}_m)}{\partial y_m^t} \right)^2 \right. \\ &\quad \left. + \left( \frac{\partial u_k(\mathbf{t}_m)}{\partial y_m^t \partial y_m^t} \right)^2 \right]^{\frac{1}{2}} \end{aligned}$$

---


$$\begin{aligned} |\mathbf{h}_k(\mathbf{t}, \mathbf{r}_k)^H \mathbf{w}|^2 &= |\mathbf{b}_k^H \mathbf{G}_k(\mathbf{t}) \mathbf{w}|^2 = \left| [\mathbf{b}_k^H \mathbf{g}_k(\mathbf{t}_1), \dots, \mathbf{b}_k^H \mathbf{g}_k(\mathbf{t}_M)] \mathbf{w} \right|^2 = \left| \sum_{m=1}^M \mathbf{b}_k^H \mathbf{g}_k(\mathbf{t}_m) w_m \right|^2 \\ &= (\mathbf{b}_k^H \mathbf{g}_k(\mathbf{t}_m) w_m + \Lambda_{k,m}) (w_m^* \mathbf{g}_k(\mathbf{t}_m)^H \mathbf{b}_k + \Lambda_{k,m}^*) \\ &= |w_m|^2 \mathbf{g}_k(\mathbf{t}_m)^H \mathbf{B}_k \mathbf{g}_k(\mathbf{t}_m) + 2\text{Re} \left\{ w_m \Lambda_{k,m}^* \mathbf{b}_k^H \mathbf{g}_k(\mathbf{t}_m) \right\} + |\Lambda_{k,m}|^2 \\ &= \sum_{i=1}^{L_k^t-1} \sum_{j=i+1}^{L_k^t} 2|w_m|^2 |\mathbf{B}_k]_{i,j}| \cos \left( \frac{2\pi}{\lambda} \mathbf{t}_m^T (-\mathbf{a}_{k,i}^t + \mathbf{a}_{k,j}^t) + \arg([\mathbf{B}_k]_{i,j}) \right) + \sum_{i=1}^{L_k^t} |w_m|^2 [\mathbf{B}_k]_{i,i} \\ &\quad + \sum_{i=1}^{L_k^t} 2|w_m| |\Lambda_{k,m}| |[\mathbf{b}_k]_i| \cos \left( \frac{2\pi}{\lambda} \mathbf{t}_m^T \mathbf{a}_{k,i}^t + \arg(w_m) - \arg(\Lambda_{k,m}) - \arg([\mathbf{b}_k]_i) \right) + |\Lambda_{k,m}|^2 \\ &= \sum_{i=1}^{L_k^t-1} \sum_{j=i+1}^{L_k^t} 2|w_m|^2 |\mathbf{B}_k]_{i,j}| \cos(\beta_{i,j,k}(\mathbf{t}_m)) + \sum_{i=1}^{L_k^t} |w_m|^2 [\mathbf{B}_k]_{i,i} \\ &\quad + \sum_{i=1}^{L_k^t} 2|w_m| |\Lambda_{k,m}| |[\mathbf{b}_k]_i| \cos(\iota_{k,i}(\mathbf{t}_m)) + |\Lambda_{k,m}|^2 \\ &\triangleq u_k(\mathbf{t}_m). \end{aligned} \quad (12)$$

$$\begin{aligned}
&\leq \left[ 4 \left( \frac{8\pi^2}{\lambda^2} \sum_{i=1}^{L_k^t-1} \sum_{j=i+1}^{L_k^t} |w_m|^2 \left| [\mathbf{B}_k]_{i,j} \right| \right. \right. \\
&\quad \left. \left. + \frac{8\pi^2}{\lambda^2} \sum_{i=1}^{L_k^t} |w_m| |\Lambda_{k,m}| \left| [\mathbf{b}_k]_i \right| \right)^2 \right]^{\frac{1}{2}} \\
&= \frac{16\pi^2}{\lambda^2} \left( \sum_{i=1}^{L_k^t-1} \sum_{j=i+1}^{L_k^t} |w_m|^2 \left| [\mathbf{B}_k]_{i,j} \right| \right. \\
&\quad \left. + \sum_{i=1}^{L_k^t} |w_m| |\Lambda_{k,m}| \left| [\mathbf{b}_k]_i \right| \right) \\
&\triangleq \bar{\psi}_{k,m}. \tag{18}
\end{aligned}$$

Since  $\bar{\psi}_{k,m} \geq \|\nabla^2 u_k(\mathbf{t}_m)\|_2$  and  $\|\nabla^2 u_k(\mathbf{t}_m)\|_2 \mathbf{I} \succeq \nabla^2 u_k(\mathbf{t}_m)$ , we have  $\bar{\psi}_{k,m} \mathbf{I} \succeq \nabla^2 u_k(\mathbf{t}_m)$ . Thus, we can choose  $\psi_{k,m}$  to be equal to  $\bar{\psi}_{k,m}$ .

With (14), a convex subset of constraint (13) is given by

$$u_k^{\text{lb},\ell}(\mathbf{t}_m) \geq \eta \gamma_k \sigma_k^2, \quad \forall k \in \mathcal{K}. \tag{19}$$

The sole remaining hurdle to solving problem (11) lies in the non-convex constraint (11d). Note that constraint (11d)

is equivalent to  $\|\mathbf{t}_m - \mathbf{t}_p\|^2 \geq D^2, \forall p \in \mathcal{M}, p \neq m$ . Since the term  $\|\mathbf{t}_m - \mathbf{t}_p\|^2$  is convex w.r.t.  $\mathbf{t}_m$ , it is lower bounded by its first-order Taylor expansion, i.e.,

$$\begin{aligned}
\|\mathbf{t}_m - \mathbf{t}_p\|^2 &\geq \|\mathbf{t}_m^\ell - \mathbf{t}_p\|^2 + 2(\mathbf{t}_m^\ell - \mathbf{t}_p)^T (\mathbf{t}_m - \mathbf{t}_m^\ell) \\
&\triangleq \mathcal{T}^{\text{lb},\ell}(\mathbf{t}_m). \tag{20}
\end{aligned}$$

By replacing  $\|\mathbf{t}_m - \mathbf{t}_p\|^2$  with  $\mathcal{T}^{\text{lb},\ell}(\mathbf{t}_m)$  and constraint (11b) with (19), we can acquire a lower bound of the optimal value of problem (11) by solving

$$\max_{\eta, \mathbf{t}_m} \eta \tag{21a}$$

$$\text{s.t. (11c), (19),} \tag{21b}$$

$$\mathcal{T}^{\text{lb},\ell}(\mathbf{t}_m) \geq D^2, \quad \forall p \in \mathcal{M}, p \neq m. \tag{21c}$$

As a convex QCP, this problem's optimal solution can be obtained readily by standard solvers (e.g., CVX [37]).

**Remark 1.** It is worth mentioning that the method proposed in [6] can also be applied to deal with the LHS of constraint (11b), i.e., the term  $|\mathbf{h}_k(\mathbf{t}, \mathbf{r}_k)^H \mathbf{w}|^2$ . However, this method necessitates a two-step approximation process to construct a lower bound for  $|\mathbf{h}_k(\mathbf{t}, \mathbf{r}_k)^H \mathbf{w}|^2$ . To be spe-

$$\begin{aligned}
\frac{\partial u_k(\mathbf{t}_m)}{\partial x_m^t} \Big|_{\mathbf{t}_m = \mathbf{t}_m^\ell} &= -\frac{4\pi}{\lambda} \sum_{i=1}^{L_k^t-1} \sum_{j=i+1}^{L_k^t} |w_m|^2 \left| [\mathbf{B}_k]_{i,j} \right| \left( -\cos \theta_{k,i}^t \sin \phi_{k,i}^t + \cos \theta_{k,j}^t \sin \phi_{k,j}^t \right) \sin(\beta_{i,j,k}(\mathbf{t}_m^\ell)) \\
&\quad - \frac{4\pi}{\lambda} \sum_{i=1}^{L_k^t} |w_m| |\Lambda_{k,m}| \left| [\mathbf{b}_k]_i \right| \cos \theta_{k,i}^t \sin \phi_{k,i}^t \sin(\iota_{k,i}(\mathbf{t}_m^\ell)), \tag{15a}
\end{aligned}$$

$$\begin{aligned}
\frac{\partial u_k(\mathbf{t}_m)}{\partial y_m^t} \Big|_{\mathbf{t}_m = \mathbf{t}_m^\ell} &= -\frac{4\pi}{\lambda} \sum_{i=1}^{L_k^t-1} \sum_{j=i+1}^{L_k^t} |w_m|^2 \left| [\mathbf{B}_k]_{i,j} \right| \left( -\sin \theta_{k,i}^t + \sin \theta_{k,j}^t \right) \sin(\beta_{i,j,k}(\mathbf{t}_m^\ell)) \\
&\quad - \frac{4\pi}{\lambda} \sum_{i=1}^{L_k^t} |w_m| |\Lambda_{k,m}| \left| [\mathbf{b}_k]_i \right| \sin \theta_{k,i}^t \sin(\iota_{k,i}(\mathbf{t}_m^\ell)). \tag{15b}
\end{aligned}$$

$$\begin{aligned}
\frac{\partial u_k(\mathbf{t}_m)}{\partial x_m^t \partial x_m^t} &= -\frac{8\pi^2}{\lambda^2} \sum_{i=1}^{L_k^t-1} \sum_{j=i+1}^{L_k^t} |w_m|^2 \left| [\mathbf{B}_k]_{i,j} \right| \left( -\cos \theta_{k,i}^t \sin \phi_{k,i}^t + \cos \theta_{k,j}^t \sin \phi_{k,j}^t \right)^2 \cos(\beta_{i,j,k}(\mathbf{t}_m)) \\
&\quad - \frac{8\pi^2}{\lambda^2} \sum_{i=1}^{L_k^t} |w_m| |\Lambda_{k,m}| \left| [\mathbf{b}_k]_i \right| \cos^2 \theta_{k,i}^t \sin^2 \phi_{k,i}^t \cos(\iota_{k,i}(\mathbf{t}_m)), \tag{17a}
\end{aligned}$$

$$\begin{aligned}
\frac{\partial u_k(\mathbf{t}_m)}{\partial x_m^t \partial y_m^t} &= \frac{\partial u_k(\mathbf{t}_m)}{\partial y_m^t \partial y_m^t} = -\frac{8\pi^2}{\lambda^2} \sum_{i=1}^{L_k^t-1} \sum_{j=i+1}^{L_k^t} |w_m|^2 \left| [\mathbf{B}_k]_{i,j} \right| \left( -\cos \theta_{k,i}^t \sin \phi_{k,i}^t + \cos \theta_{k,j}^t \sin \phi_{k,j}^t \right) \left( -\sin \theta_{k,i}^t + \sin \theta_{k,j}^t \right) \\
&\quad \times \cos(\beta_{i,j,k}(\mathbf{t}_m)) - \frac{8\pi^2}{\lambda^2} \sum_{i=1}^{L_k^t} |w_m| |\Lambda_{k,m}| \left| [\mathbf{b}_k]_i \right| \cos \theta_{k,i}^t \sin \phi_{k,i}^t \sin \theta_{k,i}^t \cos(\iota_{k,i}(\mathbf{t}_m)), \tag{17b}
\end{aligned}$$

$$\begin{aligned}
\frac{\partial u_k(\mathbf{t}_m)}{\partial y_m^t \partial y_m^t} &= -\frac{8\pi^2}{\lambda^2} \sum_{i=1}^{L_k^t-1} \sum_{j=i+1}^{L_k^t} |w_m|^2 \left| [\mathbf{B}_k]_{i,j} \right| \left( -\sin \theta_{k,i}^t + \sin \theta_{k,j}^t \right)^2 \cos(\beta_{i,j,k}(\mathbf{t}_m)) \\
&\quad - \frac{8\pi^2}{\lambda^2} \sum_{i=1}^{L_k^t} |w_m| |\Lambda_{k,m}| \left| [\mathbf{b}_k]_i \right| \sin^2 \theta_{k,i}^t \cos(\iota_{k,i}(\mathbf{t}_m)). \tag{17c}
\end{aligned}$$

cific, after expanding  $|\mathbf{h}_k(\mathbf{t}, \mathbf{r}_k)^H \mathbf{w}|^2$  as  $|\mathbf{h}_k(\mathbf{t}, \mathbf{r}_k)^H \mathbf{w}|^2 = |w_m|^2 \mathbf{g}_k(\mathbf{t}_m)^H \mathbf{B}_k \mathbf{g}_k(\mathbf{t}_m) + 2\text{Re} \left\{ w_m \Lambda_{k,m}^* \mathbf{b}_k^H \mathbf{g}_k(\mathbf{t}_m) \right\} + |\Lambda_{k,m}|^2$ , one needs to first apply the first-order Taylor expansion to the term  $|w_m|^2 \mathbf{g}_k(\mathbf{t}_m)^H \mathbf{B}_k \mathbf{g}_k(\mathbf{t}_m)$  to obtain its lower bound, followed by utilizing the second-order Taylor expansion to construct surrogate functions for the resulting lower bound and the term  $2\text{Re} \left\{ w_m \Lambda_{k,m}^* \mathbf{b}_k^H \mathbf{g}_k(\mathbf{t}_m) \right\}$ . By contrast, our proposed method requires only one approximation to obtain a surrogate lower bound of  $|\mathbf{h}_k(\mathbf{t}, \mathbf{r}_k)^H \mathbf{w}|^2$ , i.e.,  $u_k^{\text{lb}, \ell}(\mathbf{t}_m)$ . Compared with the method in [6], our proposed method not only simplifies the problem-solving process, but also is expected to be more effective in terms of the converged solution, which is validated later by the simulation results in Fig. 2 in Section V.

### C. Optimizing $\{\mathbf{r}_k\}$ for Given $\{\mathbf{w}, \{\mathbf{t}_m\}\}$

Observe that unlike  $\{\mathbf{t}_m\}$ ,  $\{\mathbf{r}_k\}$  are not coupled in the SNR expressions of the users. For this reason,  $\{\mathbf{r}_k\}$  can be collectively optimized. Given  $\{\mathbf{w}, \{\mathbf{t}_m\}\}$ , the subproblem w.r.t.  $\{\mathbf{r}_k\}$  can be written as

$$\max_{\eta, \{\mathbf{r}_k\}} \eta \quad (22a)$$

$$\text{s.t. } |\mathbf{h}_k(\mathbf{t}, \mathbf{r}_k)^H \mathbf{w}|^2 \geq \eta \gamma_k \sigma_k^2, \quad \forall k \in \mathcal{K}, \quad (22b)$$

$$(7f). \quad (22c)$$

In order to expose  $\mathbf{r}_k$  in constraint (22b), we expand  $|\mathbf{h}_k(\mathbf{t}, \mathbf{r}_k)^H \mathbf{w}|^2$  as follows:

$$\begin{aligned} & |\mathbf{h}_k(\mathbf{t}, \mathbf{r}_k)^H \mathbf{w}|^2 \\ &= \mathbf{f}_k(\mathbf{r}_k)^H \Sigma_k \mathbf{G}_k(\mathbf{t}) \mathbf{w} \mathbf{w}^H \mathbf{G}_k(\mathbf{t})^H \Sigma_k^H \mathbf{f}_k(\mathbf{r}_k) \\ &= \mathbf{f}_k(\mathbf{r}_k)^H \mathbf{C}_k \mathbf{f}_k(\mathbf{r}_k) \\ &= \sum_{i=1}^{L_k^r-1} \sum_{j=i+1}^{L_k^r} 2 \left| [\mathbf{C}_k]_{i,j} \right| \cos(\tau_{i,j}(\mathbf{r}_k)) + \sum_{i=1}^{L_k^r} [\mathbf{C}_k]_{i,i} \\ &\triangleq v(\mathbf{r}_k), \end{aligned} \quad (23)$$

where  $\mathbf{C}_k \triangleq \Sigma_k \mathbf{G}_k(\mathbf{t}) \mathbf{w} \mathbf{w}^H \mathbf{G}_k(\mathbf{t})^H \Sigma_k^H \in \mathbb{C}^{L_k^r \times L_k^r}$  and  $\tau_{i,j}(\mathbf{r}_k) \triangleq \frac{2\pi}{\lambda} \mathbf{r}_k^T \left( -\mathbf{a}_{k,i}^r + \mathbf{a}_{k,j}^r \right) + \arg([\mathbf{C}_k]_{i,j})$ . Note that  $\mathbf{C}_k$  is neither concave nor convex w.r.t.  $\mathbf{r}_k$ . Similar to (14), we can construct a second-order Taylor expansion-based concave lower bound for  $v(\mathbf{r}_k)$ , denoted by  $v^{\text{lb}, \ell}(\mathbf{r}_k)$ . We then replace  $|\mathbf{h}_k(\mathbf{t}, \mathbf{r}_k)^H \mathbf{w}|^2$  in constraint (22b) with  $v^{\text{lb}, \ell}(\mathbf{r}_k)$ , which yields the following convex QCP:

$$\max_{\eta, \{\mathbf{r}_k\}} \eta \quad (24a)$$

$$\text{s.t. } v^{\text{lb}, \ell}(\mathbf{r}_k) \geq \eta \gamma_k \sigma_k^2, \quad \forall k \in \mathcal{K}, \quad (24b)$$

$$(7f). \quad (24c)$$

Similarly, off-the-shelf solvers, such as CVX [37], can be utilized to solve problem (24) optimally.

### D. Overall Algorithm: Convergence and Complexity Analysis

Based on the above results, we outline our proposed algorithm for (P2) in Algorithm 1. It can be proved as in [39]

#### Algorithm 1 Proposed AO-based algorithm for problem (P2)

- 1: Initialize  $\{\mathbf{w}^0, \{\mathbf{t}_m^0\}, \{\mathbf{r}_k^0\}\}$  and set  $\ell = 0$ .
- 2: **repeat**
- 3:   Obtain  $\mathbf{w}^{\ell+1}$  by solving problem (10) with given  $\{\{\mathbf{t}_m^\ell\}, \{\mathbf{r}_k^\ell\}\}$ .
- 4:   **for**  $m = 1$  to  $M$  **do**
- 5:     Obtain  $\mathbf{t}_m^{\ell+1}$  by solving problem (21) with given  $\{\mathbf{w}^{\ell+1}, \mathbf{t}_1^{\ell+1}, \dots, \mathbf{t}_{m-1}^{\ell+1}, \mathbf{t}_m^\ell, \dots, \mathbf{t}_M^\ell, \{\mathbf{r}_k^\ell\}\}$ .
- 6:   **end for**
- 7:   Obtain  $\mathbf{r}_k^{\ell+1}$  by solving problem (24) with given  $\{\mathbf{w}^{\ell+1}, \{\mathbf{t}_m^{\ell+1}\}, \{\mathbf{r}_k^\ell\}\}$ .
- 8:    $\ell \leftarrow \ell + 1$ .
- 9: **until** The fractional increase of the objective value of problem (P2) between two consecutive iterations drops below a threshold  $\epsilon > 0$ .

that repeating steps 3-8 of Algorithm 1 yields a non-decreasing sequence of objective values of (P2). Furthermore, the optimal value of (P2) is upper-bounded. As a result, Algorithm 1 is assured to converge. The complexity of each iteration of this algorithm mainly arises from solving problem (10) to update  $\mathbf{w}$ , solving problem (21) to update each  $\mathbf{t}_m$ , and solving problem (24) to update  $\{\mathbf{r}_k\}$ . Since these three problems are all QCP, based on the analytical expression in [40], the complexity of solving them is given by  $\mathcal{O}(\ln \frac{1}{\epsilon} K^{1.5} M^{4.5})$ ,  $\mathcal{O}(\ln \frac{1}{\epsilon} (K + M)^{1.5})$ , and  $\mathcal{O}(\ln \frac{1}{\epsilon} K^{3.5})$ , respectively, where  $\epsilon$  is the prescribed accuracy. Hence, the overall computational complexity of Algorithm 1 is in the order of  $\mathcal{O}\left(L_1 \ln \frac{1}{\epsilon} \left(K^{1.5} M^{4.5} + M(K + M)^{1.5} + K^{3.5}\right)\right)$ , where  $L_1$  represents the number of iterations required for convergence.

## IV. MULTI-GROUP SCENARIO

In this section, we consider the general multi-group multi-cast scenario and extend the AO-based algorithm proposed in the previous section to address the corresponding problem in this challenging setup.

### A. Optimizing $\{\mathbf{w}_n\}$ for Given $\{\{\mathbf{t}_m\}, \{\mathbf{r}_k\}\}$

Given any fixed  $\{\{\mathbf{t}_m\}, \{\mathbf{r}_k\}\}$ , and recalling that we defined  $\mathbf{H}_k(\mathbf{t}, \mathbf{r}_k) \triangleq \mathbf{h}_k(\mathbf{t}, \mathbf{r}_k) \mathbf{h}_k(\mathbf{t}, \mathbf{r}_k)^H$  in Section III-A, the subproblem of (P1) regarding to  $\{\mathbf{w}_n\}$  can be expressed as

$$\max_{\eta, \{\mathbf{w}_n\}} \eta \quad (25a)$$

$$\text{s.t. } \frac{1}{\gamma_k} \frac{\mathbf{w}_n^H \mathbf{H}_k(\mathbf{t}, \mathbf{r}_k) \mathbf{w}_n}{\eta} \geq \sum_{q=1, q \neq n}^N \mathbf{w}_q^H \mathbf{H}_k(\mathbf{t}, \mathbf{r}_k) \mathbf{w}_q + \sigma_k^2, \quad (25b)$$

$$\forall k \in \mathcal{G}_n, n \in \mathcal{N}, \quad (25c)$$

$$(7c). \quad (25c)$$

Note that the convexity of  $\frac{\mathbf{w}_n^H \mathbf{H}_k(\mathbf{t}, \mathbf{r}_k) \mathbf{w}_n}{\eta}$  results in the non-convexity of constraint (25b). This prompts us to approximate  $\frac{\mathbf{w}_n^H \mathbf{H}_k(\mathbf{t}, \mathbf{r}_k) \mathbf{w}_n}{\eta}$  by its first-order Taylor expansion-based affine under-estimator, yielding

$$\max_{\eta, \{\mathbf{w}_n\}} \eta \quad (26a)$$

$$\begin{aligned} \text{s.t. } \frac{1}{\gamma_k} \mathcal{F}^{\text{lb},r}(\mathbf{w}_n) &\geq \sum_{q=1, q \neq n}^N \mathbf{w}_q^H \mathbf{H}_k(\mathbf{t}, \mathbf{r}_k) \mathbf{w}_q + \sigma_k^2, \\ \forall k \in \mathcal{G}_n, n \in \mathcal{N}, & \end{aligned} \quad (26b)$$

$$(7c), \quad (26c)$$

where

$$\begin{aligned} \mathcal{F}^{\text{lb},r}(\mathbf{w}_n) &\triangleq \frac{2\text{Re}\left\{(\mathbf{w}_n^r)^H \mathbf{H}_k(\mathbf{t}, \mathbf{r}_k) \mathbf{w}_n\right\}}{\eta^r} \\ &\quad - \frac{(\mathbf{w}_n^r)^H \mathbf{H}_k(\mathbf{t}, \mathbf{r}_k) \mathbf{w}_n^r}{(\eta^r)^2} \end{aligned} \quad (27)$$

with  $\mathbf{w}_n^r$  and  $\eta^r$  being the given local points in the  $r$ -th iteration. By solving the convex QCP in (26) via standard solvers such as CVX [37], we obtain a performance lower bound of problem (25).

### B. Optimizing $\mathbf{t}_m$ for Given $\{\{\mathbf{w}_n\}, \{\mathbf{t}_p\}_{p \in \mathcal{M} \setminus \{m\}}, \{\mathbf{r}_k\}\}$

With fixed  $\{\{\mathbf{w}_n\}, \{\mathbf{t}_p\}_{p \in \mathcal{M} \setminus \{m\}}, \{\mathbf{r}_k\}\}$ , (P1) reduces to

$$\max_{\eta, \mathbf{t}_m} \eta \quad (28a)$$

$$\begin{aligned} \text{s.t. } \frac{1}{\gamma_k} \frac{|\mathbf{h}_k(\mathbf{t}, \mathbf{r}_k)^H \mathbf{w}_n|^2}{\sum_{q=1, q \neq n}^N |\mathbf{h}_k(\mathbf{t}, \mathbf{r}_k)^H \mathbf{w}_q|^2 + \sigma_k^2} &\geq \eta, \\ \forall k \in \mathcal{G}_n, n \in \mathcal{N}, & \end{aligned} \quad (28b)$$

$$\mathbf{t}_m \in \mathcal{C}^t, \quad (28c)$$

$$\|\mathbf{t}_m - \mathbf{t}_p\| \geq D, \quad \forall p \in \mathcal{M}, p \neq m. \quad (28d)$$

Similar to (12),  $|\mathbf{h}_k(\mathbf{t}, \mathbf{r}_k)^H \mathbf{w}_n|^2$  in constraint (28b) can be expanded as

$$\begin{aligned} &|\mathbf{h}_k(\mathbf{t}, \mathbf{r}_k)^H \mathbf{w}_n|^2 \\ &= \sum_{i=1}^{L_k^t-1} \sum_{j=i+1}^{L_k^t} 2|w_{n,m}|^2 \left| [\mathbf{B}_k]_{i,j} \right| \cos(\beta_{i,j,k}(\mathbf{t}_m)) \\ &\quad + \sum_{i=1}^{L_k^t} |w_{n,m}|^2 \left| [\mathbf{B}_k]_{i,i} \right| + |\Lambda_{k,n,m}|^2 \\ &\quad + \sum_{i=1}^{L_k^t} 2|w_{n,m}| \left| \Lambda_{k,n,m} \right| \left| [\mathbf{b}_k]_i \right| \cos(\iota_{k,i,n}(\mathbf{t}_m)) \\ &\triangleq u_{k,n}(\mathbf{t}_m), \end{aligned} \quad (29)$$

where  $\mathbf{B}_k$  and  $\beta_{i,j,k}(\mathbf{t}_m)$  are defined in Section III-B,  $w_{n,m}$  is the  $m$ -th element of  $\mathbf{w}_n$ ,  $\Lambda_{k,n,m} \triangleq \sum_{p=1, p \neq m}^M \mathbf{b}_k^H \mathbf{g}_k(\mathbf{t}_p) w_{n,p}$ , and  $\iota_{k,i,n}(\mathbf{t}_m) \triangleq \frac{2\pi}{\lambda} \mathbf{t}_m^T \mathbf{a}_{k,i}^t + \arg(w_{n,m}) - \arg(\Lambda_{k,n,m}) - \arg([\mathbf{b}_k]_i)$ . With (29), constraint (28b) can be recast as

$$\frac{1}{\gamma_k} \frac{u_{k,n}(\mathbf{t}_m)}{\sum_{q=1, q \neq n}^N u_{k,q}(\mathbf{t}_m) + \sigma_k^2} \geq \eta, \quad \forall k \in \mathcal{G}_n, n \in \mathcal{N}, \quad (30)$$

where the expression of  $u_{k,q}(\mathbf{t}_m)$  can be obtained by replacing the index “ $n$ ” in (29) with “ $q$ ”. Note that  $u_{k,n}(\mathbf{t}_m)$  and  $u_{k,q}(\mathbf{t}_m)$  are neither concave nor convex, and the same applies to  $\frac{u_{k,n}(\mathbf{t}_m)}{\eta}$ . If we rewrite constraint (30) as  $\frac{1}{\gamma_k} \frac{u_{k,n}(\mathbf{t}_m)}{\eta} \geq \sum_{q=1, q \neq n}^N u_{k,q}(\mathbf{t}_m) + \sigma_k^2, \forall k \in \mathcal{G}_n, n \in \mathcal{N}$ , which is in the same form as constraint (25b) in the previous subsection, the

resulting constraint is still intractable. To address this issue, we introduce slack variables  $\{z_k\}$  and convert (30) to

$$\frac{1}{\gamma_k} u_{k,n}(\mathbf{t}_m) \geq \eta z_k, \quad \forall k \in \mathcal{G}_n, n \in \mathcal{N}, \quad (31a)$$

$$\sum_{q=1, q \neq n}^N u_{k,q}(\mathbf{t}_m) + \sigma_k^2 \leq z_k, \quad \forall k \in \mathcal{G}_n, n \in \mathcal{N}. \quad (31b)$$

The equivalence between (30) and (31) can be verified by contradiction. However, the constraints in (31) are still non-convex. We first deal with (31a). Similar to (14), with the given local point  $\mathbf{t}_m^r$  in the  $r$ -th iteration, we construct a concave lower-bound surrogate function, denoted by  $u_{k,n}^{\text{lb},r}(\mathbf{t}_m)$ , for the LHS of (31a). For the right-hand-side of (31a), it is not jointly convex w.r.t.  $\eta$  and  $z_k$  but satisfies [38, (101)]:

$$\eta z_k \leq \frac{1}{2} \left( \frac{z_k^r}{\eta^r} \eta^2 + \frac{\eta^r}{z_k^r} z_k^2 \right) \triangleq \chi^{\text{ub},r}(\eta, z_k), \quad (32)$$

where  $\eta^r$  and  $z_k^r$  are the given local points in the  $r$ -th iteration. Then, a convex approximation of constraint (31a) can be established immediately, given by

$$\frac{1}{\gamma_k} u_{k,n}^{\text{lb},r}(\mathbf{t}_m) \geq \chi^{\text{ub},r}(\eta, z_k), \quad \forall k \in \mathcal{G}_n, n \in \mathcal{N}. \quad (33)$$

To proceed, we tackle the non-convex constraint (31b). As we need to construct an upper bound for  $u_{k,q}(\mathbf{t}_m)$ , the inequality in (14) is not applicable. Nevertheless, according to [38, Lemma 12], we have

$$\begin{aligned} u_{k,q}(\mathbf{t}_m) &\leq u_{k,q}(\mathbf{t}_m^r) + \nabla u_{k,q}(\mathbf{t}_m^r)^T (\mathbf{t}_m - \mathbf{t}_m^r) \\ &\quad + \frac{\psi_{k,q,m}}{2} (\mathbf{t}_m - \mathbf{t}_m^r)^T (\mathbf{t}_m - \mathbf{t}_m^r) \\ &\triangleq u_{k,q}^{\text{ub},r}(\mathbf{t}_m), \end{aligned} \quad (34)$$

where  $\psi_{k,q,m}$  is a positive real number satisfying  $\psi_{k,q,m} \mathbf{I} \succeq \nabla^2 u_{k,q}(\mathbf{t}_m)$  and can be determined by following similar steps as in (18). Subsequently, constraint (31b) can be approximated as

$$\sum_{q=1, q \neq n}^N u_{k,q}^{\text{ub},r}(\mathbf{t}_m) + \sigma_k^2 \leq z_k, \quad \forall k \in \mathcal{G}_n, n \in \mathcal{N}, \quad (35)$$

which is a convex constraint.

Now, the only barrier left in solving problem (28) is the non-convex constraint (28d), which is exactly the same as constraint (11d). Recall that in Section III-B, we approximated constraint (11d) as a convex one, which can be expressed as

$$\mathcal{T}^{\text{lb},r}(\mathbf{t}_m) \geq D^2, \quad \forall p \in \mathcal{M}, p \neq m, \quad (36)$$

where the expression of  $\mathcal{T}^{\text{lb},r}(\mathbf{t}_m)$  can be obtained by replacing the index “ $\ell$ ” in (20) with “ $r$ ”. Consequently, by replacing constraint (28b) with (33) and (35), and replacing constraint (28d) with (36), we arrive at the following problem:

$$\max_{\eta, \mathbf{t}_m, \{z_k\}} \eta \quad (37a)$$

$$\text{s.t. } (28c), (33), (35), (36). \quad (37b)$$

Note that problem (37) is a convex QCP that can be optimally solved using CVX [37], and its optimal value serves as a lower



bound of that of problem (28).

### C. Optimizing $\{\mathbf{r}_k\}$ for Given $\{\mathbf{w}, \{\mathbf{t}_m\}\}$

When given other variables,  $\{\mathbf{r}_k\}$  can be optimized by solving the following subproblem:

$$\max_{\eta, \{\mathbf{r}_k\}} \eta \quad (38a)$$

$$\text{s.t.} \quad \frac{1}{\gamma_k} \frac{|\mathbf{h}_k(\mathbf{t}, \mathbf{r}_k)^H \mathbf{w}_n|^2}{\sum_{q=1, q \neq n}^N |\mathbf{h}_k(\mathbf{t}, \mathbf{r}_k)^H \mathbf{w}_q|^2 + \sigma_k^2} \geq \eta, \quad (38b)$$

$$\forall k \in \mathcal{G}_n, n \in \mathcal{N}, \quad (7e). \quad (38c)$$

As in (23), we can express the term  $|\mathbf{h}_k(\mathbf{t}, \mathbf{r}_k)^H \mathbf{w}_n|^2$  as

$$\begin{aligned} & |\mathbf{h}_k(\mathbf{t}, \mathbf{r}_k)^H \mathbf{w}_n|^2 \\ &= \sum_{i=1}^{L_k^t-1} \sum_{j=i+1}^{L_k^r} 2 \left| [\mathbf{C}_{k,n}]_{i,j} \right| \cos(\tau_{i,j,n}(\mathbf{r}_k)) + \sum_{i=1}^{L_k^r} [\mathbf{C}_{k,n}]_{i,i} \\ &\triangleq v_n(\mathbf{r}_k), \end{aligned} \quad (39)$$

where  $\mathbf{C}_{k,n} \triangleq \sum_k \mathbf{G}_k(\mathbf{t}) \mathbf{w}_n \mathbf{w}_n^H \mathbf{G}_k(\mathbf{t})^H \sum_k^H \in \mathbb{C}^{L_k^t \times L_k^r}$  and  $\tau_{i,j,n}(\mathbf{r}_k) \triangleq \frac{2\pi}{\lambda} \mathbf{r}_k^T (-\mathbf{a}_{k,i}^r + \mathbf{a}_{k,j}^t) + \arg([\mathbf{C}_{k,n}]_{i,j})$ . Also, replacing the index “ $n$ ” with “ $q$ ” in (39), we can obtain the expansion of  $|\mathbf{h}_k(\mathbf{t}, \mathbf{r}_k)^H \mathbf{w}_q|^2$ , i.e.,  $v_q(\mathbf{r}_k)$ . Then, constraint (38b) can be transformed into

$$\frac{1}{\gamma_k} \frac{v_n(\mathbf{r}_k)}{\sum_{q=1, q \neq n}^N v_q(\mathbf{r}_k) + \sigma_k^2} \geq \eta, \quad \forall k \in \mathcal{G}_n, n \in \mathcal{N}. \quad (40)$$

Since constraint (40) shares a similar structure with constraint (30), it can be addressed in the same manner as for (30), which is thus omitted for brevity. After replacing constraint (38b) with the convex approximation of constraint (40), a lower bound of the optimal value of the subproblem (38) can be obtained by solving the resulting convex QCP.

### D. Overall Algorithm: Convergence and Complexity Analysis

The detailed steps of the proposed algorithm for (P1) are not provided here, as they closely resemble those outlined in Algorithm 1 for (P2). Moreover, the convergence of this algorithm is assured for identical reasons to Algorithm 1. Besides, in each iteration of this algorithm, the complexity of updating  $\{\mathbf{w}_n\}$ ,  $\mathbf{t}_m$ , and  $\{\mathbf{r}_k\}$  by solving the corresponding subproblems is given by  $\mathcal{O}(\ln \frac{1}{\epsilon} K^{1.5} M^3 N^3)$ ,  $\mathcal{O}(\ln \frac{1}{\epsilon} K^2 (K+M)^{1.5})$ , and  $\mathcal{O}(\ln \frac{1}{\epsilon} K^{3.5})$ , respectively, with  $\epsilon$  representing the solution accuracy [40]. Thus, the total computational complexity of this algorithm is about  $\mathcal{O}(L_2 \ln \frac{1}{\epsilon} (K^{1.5} M^3 N^3 + MK^2 (K+M)^{1.5} + K^{3.5}))$  with  $L_2$  standing for the number of iterations needed for convergence.

## V. SIMULATION RESULTS

This section provides numerical examples to validate the effectiveness of our proposed algorithm. We assume that the users are randomly dispersed around the BS. The distance between user  $k$  and the BS, denoted by  $d_k$  in meter (m), is

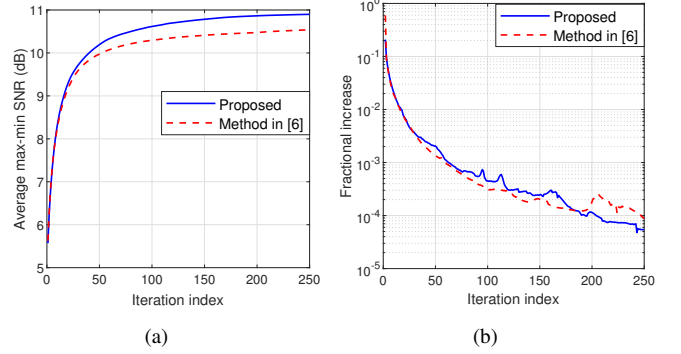


Fig. 2. Convergence behaviors of the proposed Algorithm 1 and the existing method in [6]. (a) Average max-min SNR versus the iteration index; (b) The corresponding fractional increase of the max-min SNR versus the iteration index.

uniformly distributed over  $[20, 60]$ . We adopt the geometry channel model, where the numbers of transmit and receive channel paths for each user are identical, i.e.,  $L_k^t = L_k^r \triangleq L$ ,  $\forall k \in \mathcal{K}$ . Under this condition, the path-response matrix for each user is diagonal, i.e.,  $\sum_k = \text{diag}\{\sigma_{k,1}, \dots, \sigma_{k,L}\}$  with  $\sigma_{k,\ell}$  satisfying  $\sigma_{k,\ell} \sim \mathcal{CN}(0, \frac{c_k^2}{L})$ ,  $\ell = 1, \dots, L$  [19]. Moreover,  $c_k^2 = C_0 d_k^{-\alpha}$ , where  $C_0 = -40$  dB is the expected average channel power gain at the reference distance of 1 m and  $\alpha = 2.8$  denotes the path-loss exponent. The elevation and azimuth AoDs/AoAs of the channel paths for each user are assumed to be independent and identically distributed variables, following a uniform distribution over  $[-\frac{\pi}{2}, \frac{\pi}{2}]$ . The moving regions for the transmit/receive MAs are set as  $\mathcal{C}^t = \mathcal{C}_k^r = [-\frac{A}{2}, \frac{A}{2}] \times [-\frac{A}{2}, \frac{A}{2}]$ ,  $\forall k \in \mathcal{K}$ . Besides, we set  $M = 4$ ,  $D = \frac{\lambda}{2}$ ,  $\sigma_k^2 = -80$  dBm, and  $\gamma_k = 1$  for all  $k \in \mathcal{K}$  (i.e., considering the max-min SNR/SINR). The values of  $P_{\max}$ ,  $A$ ,  $L$ ,  $K$  and  $N$  will be specified in the following simulations.

### A. Single-Group Scenario

For the single-group scenario, we first illustrate the convergence performance of our proposed Algorithm 1 and compare it with the method based on two-step approximations in [6], as shown in Fig. 2. Here, we set  $P_{\max} = 15$  dBm,  $L = 10$ ,  $A = 3\lambda$ , and  $K = 6$ . In Fig. 2(a), we observe that the max-min SNR obtained by both algorithms increases with the iteration index, showing particularly rapid growth during the early iterations. Meanwhile, Fig. 2(b) demonstrates a general decreasing trend in the fractional increase of the obtained max-min SNR as the iteration index progresses. Combining Figs. 2(a) and 2(b), it can be seen that Algorithm 1, given the threshold  $\epsilon$  defined therein, is guaranteed to terminate after a finite number of iterations. If we set  $\epsilon = 10^{-4}$ , Algorithm 1 converges earlier than the method in [6], yet achieves a superior solution. This is expected since Algorithm 1 makes only one approximation while the method in [6] utilizes two.

Next, we compare the achievable max-min SNR of our proposed Algorithm 1 with those of the following four benchmark schemes: 1) **Receive MA**: the BS is equipped with a uniform linear array (ULA) comprising  $M$  FPAs, spaced by

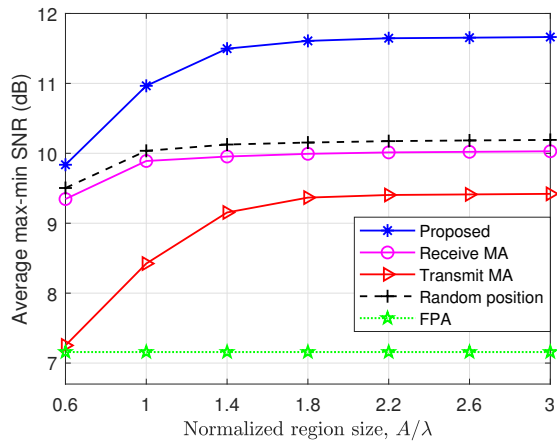


Fig. 3. Average max-min SNR versus the normalized region size.

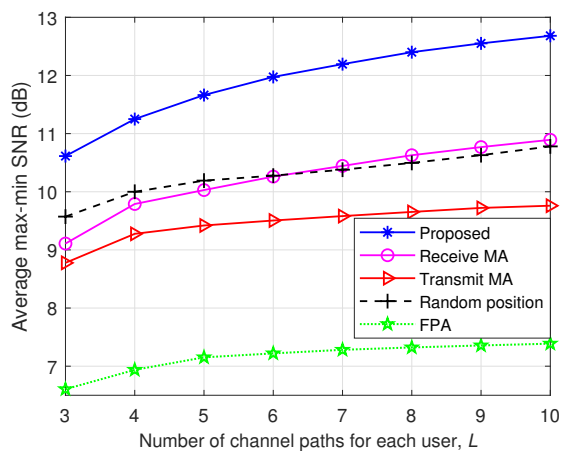


Fig. 4. Average max-min SNR versus the number of paths for each user.

$\frac{\lambda}{2}$ , while each user employs an MA; 2) **Transmit MA**: the BS is equipped with  $M$  MAs, while the antenna at user  $k$  remains fixed at the reference point  $\mathbf{o}_k^r = [0, 0]^T, \forall k \in \mathcal{K}$ ; 3) **FPA**: the  $M$  antennas at the BS and the single antenna at each user are all FPAs; 4) **Random position**: in each channel realization, we generate 100 samples of  $\{\{\mathbf{t}_m\}, \{\mathbf{r}_k\}\}$  randomly and independently. For each position sample,  $\{\{\mathbf{t}_m\}, \{\mathbf{r}_k\}\}$  satisfy constraints (7d)-(7f) and the transmit beamforming is optimized under given  $\{\{\mathbf{t}_m\}, \{\mathbf{r}_k\}\}$ . We select the best-performing solution among these 100 samples as the output of this scheme.

In Fig. 3, we plot the max-min SNR obtained by different schemes versus the normalized region size  $A/\lambda$  when  $P_{\max} = 15$  dBm,  $L = 5$ , and  $K = 3$ . Firstly, it is observed that as  $A/\lambda$  increases from a small value, the achieved max-min SNR of all the schemes, except for the FPA scheme, exhibits a monotonic growth. This is attributed to the enhanced flexibility in designing the MA positions within the enlarged regions, leading to a potential performance enhancement. However, beyond a certain threshold of  $A/\lambda$ , further increases do not bring performance improvements. This suggests that the maximum achievable max-min SNR is practically attainable within finite transmit and/or receive regions. Secondly, it

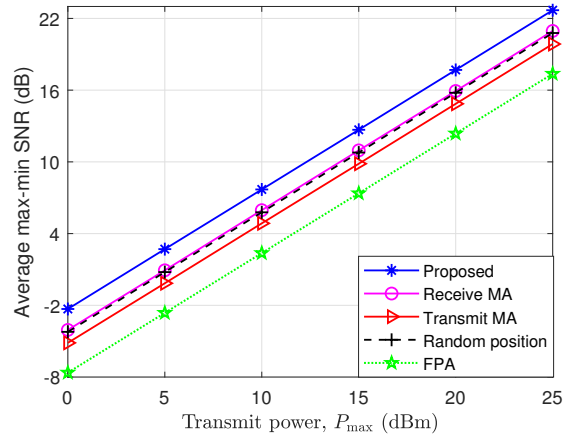


Fig. 5. Average max-min SNR versus the maximum transmit power at the BS.

appears that the max-min SNR achieved by the proposed and transmit MA schemes becomes saturated later than that of the receive MA scheme. In other words, compared to each receive MA, the transmit MAs require a larger moving region to achieve their potential maximum performance. This is because each receive MA has its own moving region, while the  $M$  transmit MAs share a single moving region and are constrained by the minimum distance requirement. Thirdly, the three schemes employing transmit and/or receive MAs demonstrate significantly better performance than the FPA scheme. This is anticipated as the MAs can be strategically placed to improve the channel conditions of the users, especially those with relatively poor channel conditions, consequently enhancing the max-min SNR performance. Finally, our proposed algorithm consistently achieves the highest max-min SNR since it exploits the most spatial DoFs to enhance the system performance. Take the case with  $A/\lambda = 3$  as an example, the proposed algorithm demonstrates approximately 14.4%, 16.3%, 23.8%, and 62.9% performance improvement over the random position, receive MA, transmit MA, and FPA schemes, respectively.

Fig. 4 depicts the max-min SNR versus the number of channel paths  $L$  for each user when  $P_{\max} = 15$  dBm,  $A = 3\lambda$ , and  $K = 3$ . It is first observed that with the increase in  $L$ , all the schemes, including the FPA scheme, exhibit an enhancement in max-min SNR. This improvement is ascribed to the heightened spatial diversity with increased  $L$ . Additionally, the MAs can augment spatial diversity further by adjusting their positions within the given moving regions. This is the reason why the max-min SNR experiences a more pronounced increase with  $L$  for the four schemes employing MAs compared to the FPA scheme. We also note that the performance of the receive MA scheme surpasses that of the random position scheme when  $L$  becomes larger. This is because the receive MA scheme can more effectively capitalize on the enhanced spatial diversity resulting from the larger  $L$  by properly placing the receive MAs. As a consequence, it achieves greater performance gains compared to the random position scheme, where the MAs are randomly placed.

In Fig. 5, we illustrate the max-min SNR of the proposed

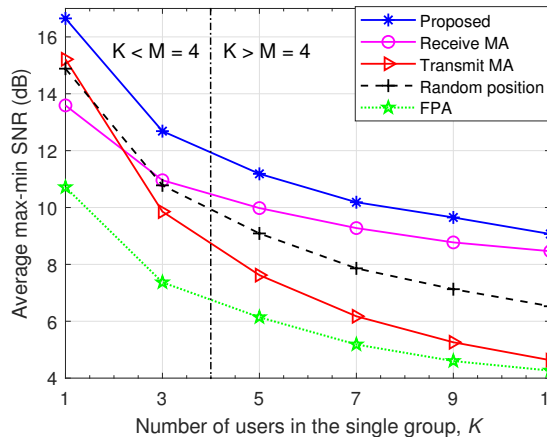
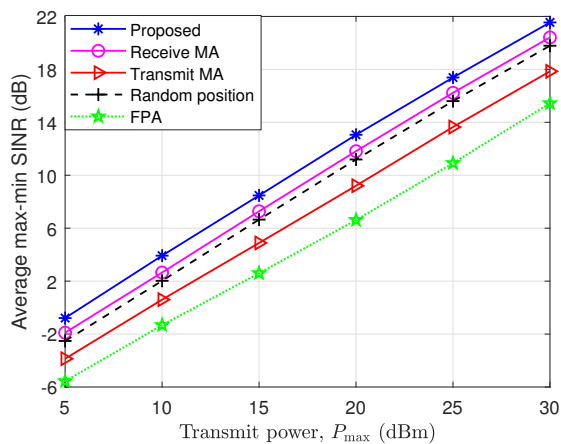
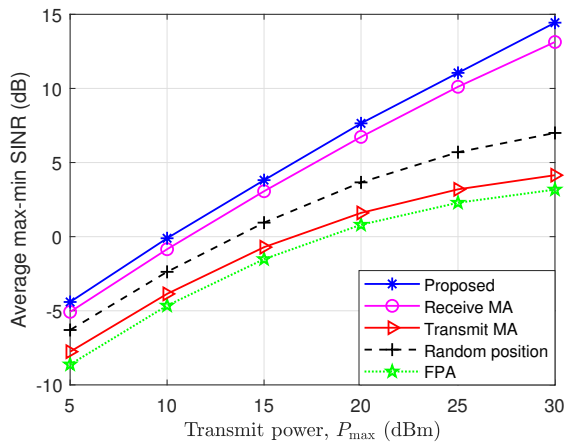


Fig. 6. Average max-min SINR versus the number of users in the single group.



(a)  $K = 4$ ,  $N = 2$ , and  $|\mathcal{G}_1| = |\mathcal{G}_2| = 2$ .



(b)  $K = 9$ ,  $N = 3$ , and  $|\mathcal{G}_1| = |\mathcal{G}_2| = |\mathcal{G}_3| = 3$ .

Fig. 7. Average max-min SINR versus the maximum transmit power at the BS.

and benchmark schemes versus the maximum transmit power at the BS when  $L = 10$ ,  $A = 3\lambda$ , and  $K = 3$ . As evident, the proposed algorithm can achieve a certain level of performance with reduced transmit power compared to other schemes. For instance, to attain a max-min SINR of 10 dB, the proposed

algorithm requires only about 12 dBm transmit power, whereas the receive MA, random position, transmit MA, and FPA schemes need about 14, 14, 15, and 17.5 dBm, respectively. It is also noteworthy that the achieved max-min SINR of all the schemes linearly increases with a slope of about 1 as  $P_{\max}$  increases. This is because all the users experience an interference-free stream in the single-group multicast scenario. However, things can be different in the multi-group multicast scenario, which will be clarified in the next subsection.

Fig. 6 investigates the impact of the number of users  $K$  on the performance of different schemes when  $P_{\max} = 15$  dBm,  $L = 10$ , and  $A = 4\lambda$ . Interestingly, it is observed that when  $M$  is slightly greater than  $K$  (i.e., when  $M = 4$  and  $K = 3$ ), the receive MA scheme achieves a higher max-min SINR than the transmit MA scheme, despite the receive MAs being at a numerical disadvantage compared to the transmit MAs. This is primarily because, in the receive MA scheme, all users can achieve their individual maximum SNR simultaneously by adjusting the receive MAs to positions that yield higher channel gains and/or increased correlation among user channel vectors within the same group. In contrast, in the transmit MA scheme, the users are always competing for resources, and the positioning of the transmit MAs requires consideration of the trade-offs among the channel conditions of all users. As such, the receive MA scheme outperforms the transmit MA scheme, even though the transmit MAs are slightly outnumbered. Furthermore, with the increase of  $K$ , the gap between the curves representing the receive MA and transmit MA schemes widens. This happens because the number of transmit MAs remains constant, while the number of receive MAs increases with  $K$ . As  $K$  increases, it becomes increasingly difficult for the transmit MAs to maintain performance fairness among different users. Nevertheless, it remains feasible for all users to achieve their individual maximum SNR with the aid of receive MAs.

### B. Multi-Group Scenario

This subsection considers the multi-group scenario and compares the performance of our proposed algorithm with the four benchmark schemes defined in the previous subsection.

In Fig. 7, we plot the max-min SINR versus the transmit power at the BS when  $L = 10$  and  $A = 4\lambda$ . Two setups are considered: one with  $K = 4$ ,  $N = 2$ , and  $|\mathcal{G}_1| = |\mathcal{G}_2| = 2$  (Fig. 7(a)), and the other with  $K = 9$ ,  $N = 3$ , and  $|\mathcal{G}_1| = |\mathcal{G}_2| = |\mathcal{G}_3| = 3$  (Fig. 7(b)). From Fig. 7(a), it is observed that as  $P_{\max}$  increases, all the curves, including the one representing the FPA scheme, do not show a deceleration in growth rate or signs of saturation. This is in line with the result in [41], which indicates that if the number of transmit antennas  $M$  satisfies the condition:  $M \geq 1 + K - \min_{n \in \mathcal{N}} |\mathcal{G}_n|$ , classical beamforming enables each beam to be placed in the null space of all its unintended groups. As such, each multicast group can receive an interference-free stream. However, the simulation setup of Fig. 7(b) violates the condition that  $M \geq 1 + K - \min_{n \in \mathcal{N}} |\mathcal{G}_n|$ . Therefore, as the inter-group interference increases with  $P_{\max}$ , the max-min SINR achieved by the FPA scheme tends to saturate. In contrast, the max-min SINR of the proposed algorithm exhibits an almost linear

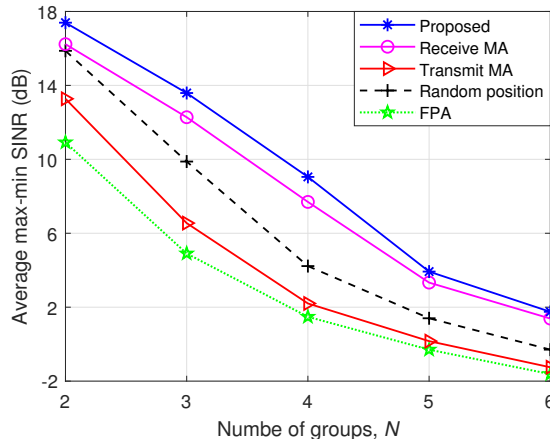


Fig. 8. Average max-min SINR versus the number of groups.

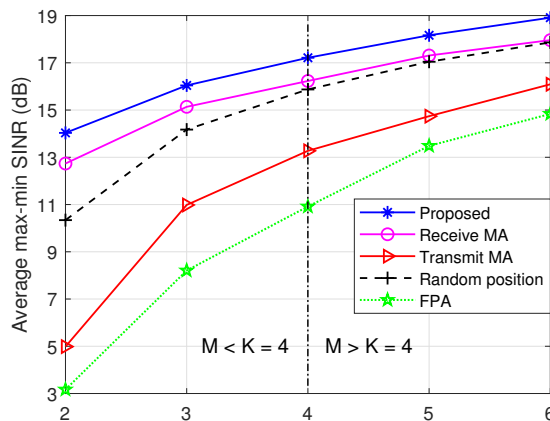


Fig. 9. Average max-min SINR versus the number of transmit MAs at the BS.

increase with the growth of  $P_{\max}$  in both Fig. 7(a) and Fig. 7(b), significantly surpassing that of the FPA scheme. This superiority can be attributed to the advantages of MAs, which not only enhance the channel gain but also mitigate inter-group interference more effectively compared to the FPAs. Besides, we note that the receive MA scheme performs much better than the transmit MA scheme, with the performance gain being more pronounced in Fig. 7(b) compared to that in Fig. 7(a). This suggests that when  $K \geq M$ , receive MAs are more effective in improving max-min fairness than transmit MAs, and the larger the gap between  $K$  and  $M$ , the more obvious it is. This aligns with the conclusion drawn from Fig. 6.

Fig. 8 illustrates the max-min SINR achieved by different schemes versus the number of groups when  $P_{\max} = 25$  dBm,  $L = 10$ , and  $A = 4\lambda$ . Here, we assume that each group consists of 2 users, i.e.,  $|\mathcal{G}_n| = 2, \forall n \in \mathcal{N}$ . It is observed that there is a significant decrease in the achieved max-min SINR with increasing  $N$  for all schemes. This is intuitive since a greater number of groups makes it more difficult to mitigate inter-group interference. Particularly, based on the DoF analysis in [41], the MMF-DoF achieved by classical beamforming with FPAs decreases from 1 to 0 when  $N$

increases from 2 to 3. Thus, the polyline representing the FPA scheme displays the steepest slope during the transition from  $N = 2$  to  $N = 3$ , compared to other variations in  $N$ . By contrast, the steepest slope for the proposed algorithm occurs during the transition from  $N = 4$  to  $N = 5$ . The reason lies in the proposed algorithm's ability to leverage the diversity gain and the interference mitigation gain in the spatial domain by adjusting the positions of both transmit and receive MAs. This feature makes it very likely for the proposed algorithm to have positive MMF-DoF values even when  $N = 3$  and  $N = 4$ . It is also noteworthy that when  $N \geq 5$  (i.e.,  $K \geq 5 \times 2 = 10$ ), the performance gap between the receive MA and FPA schemes, as well as that between the proposed and receive MA schemes, becomes marginal. This again suggests that when  $K$  far exceeds  $M$ , the performance gain from moving the transmit MAs is minor and much smaller than that from moving the receive MAs.

The effect of the number of transmit MAs,  $M$ , on the performance of different schemes is shown in Fig. 9. Other parameters are set as:  $P_{\max} = 25$  dBm,  $L = 10$ ,  $A = 4\lambda$ ,  $K = 4$ ,  $N = 2$ , and  $|\mathcal{G}_1| = |\mathcal{G}_2| = 2$ . It is shown that the increase in  $M$  results in an augmentation of the max-min SINR achieved by all the schemes. This is expected as the additional antennas introduce more DoFs, allowing the BS to form sharp beams directed toward the desired users to improve the desired signal power with less co-channel interference. Moreover, the proposed algorithm outperforms the others under any value of  $M$ . When  $M = 5$ , for instance, the max-min SINR of the proposed algorithm increases by 5.0%, 6.6%, 23.3%, and 34.7% compared to those of the receive MA, random position, transmit MA, and FPA schemes, respectively. Also, the proposed algorithm requires fewer transmit antennas than other schemes to achieve a certain level of max-min SINR performance due to its higher flexibility in MA positioning. Lastly, when  $M$  slightly exceeds  $K$ , the receive MA scheme still performs better than the transmit MA scheme, which is in consistent with the observation from Fig. 6.

## VI. CONCLUSION

In this paper, we investigated a novel MA-enhanced multicast communication system. Aiming to maximize the minimum weighted SINR among all the users, we formulated a design problem, where the position of each transmit/receive MA and the transmit precoders at the BS were jointly optimized. Despite the non-convex nature of the considered problem with highly coupled optimization variables, we proposed an efficient AO-based algorithm initially customized for the single-group scenario, which was then extended to the general multi-group scenario. Our proposed algorithm was validated through simulations, demonstrating its effectiveness and offering useful engineering insights. Firstly, MAs can remarkably improve the max-min SNR/SINR performance compared to the case with FPAs, as they enable higher spatial diversity and multiplexing gains by exploiting additional DoFs within the continuous spatial domain. Secondly, compared to benchmark schemes, the proposed algorithm achieves a significant reduction in the necessary transmit power or number of antennas to attain



a target level of max-min SNR/SINR performance. Thirdly, under the assumption that the transmit region and each receive region have identical sizes, employing only receive MAs outperforms employing only transmit MAs in terms of max-min SNR/SINR when  $K \geq M$ . And, this remains true even when  $M$  is slightly greater than  $K$ .

#### REFERENCES

- [1] S. A. Busari, K. M. S. Huq, S. Mumtaz, L. Dai, and J. Rodriguez, "Millimeter-wave massive MIMO communication for future wireless systems: A survey," *IEEE Commun. Surveys Tuts.*, vol. 20, no. 2, pp. 836–869, 2nd Quart. 2017.
- [2] E. Telatar, "Capacity of multi-antenna gaussian channels," *European Trans. Telecommun.*, vol. 10, no. 6, pp. 585–595, Nov. 1999.
- [3] A. J. Paulraj, D. A. Gore, R. U. Nabar, and H. Bolcskei, "An overview of MIMO communications—a key to gigabit wireless," *Proc. IEEE*, vol. 92, no. 2, pp. 198–218, Feb. 2004.
- [4] A. Goldsmith, S. A. Jafar, N. Jindal, and S. Vishwanath, "Capacity limits of MIMO channels," *IEEE J. Sel. Areas Commun.*, vol. 21, no. 5, pp. 684–702, Jun. 2003.
- [5] L. Zhu, W. Ma, and R. Zhang, "Modeling and performance analysis for movable antenna enabled wireless communications," *IEEE Trans. Wireless Commun.*, Nov. 2023, early access, doi: 10.1109/TWC.2023.3330887.
- [6] W. Ma, L. Zhu, and R. Zhang, "MIMO capacity characterization for movable antenna systems," *IEEE Trans. Wireless Commun.*, Sep. 2023, early access, doi:10.1109/TWC.2023.3307696.
- [7] L. Zhu, W. Ma, and R. Zhang, "Movable antennas for wireless communication: Opportunities and challenges," *IEEE Commun. Mag.*, Oct. 2023, early access, doi: 10.1109/MCOM.001.2300212.
- [8] K.-K. Wong, A. Shojaefard, K.-F. Tong, and Y. Zhang, "Fluid antenna systems," *IEEE Trans. Wireless Commun.*, Mar. 2021.
- [9] K. K. Wong, A. Shojaefard, K.-F. Tong, and Y. Zhang, "Performance limits of fluid antenna systems," *IEEE Commun. Lett.*, vol. 24, no. 11, pp. 2469–2472, Nov. 2020.
- [10] A. F. Molisch and M. Z. Win, "MIMO systems with antenna selection," *IEEE Microwave Mag.*, vol. 5, no. 1, pp. 46–56, Mar. 2004.
- [11] S. Sanayei and A. Nosratinia, "Antenna selection in MIMO systems," *IEEE Commun. Mag.*, vol. 42, no. 10, pp. 68–73, Oct. 2004.
- [12] X. Chen, B. Feng, Y. Wu, D. W. K. Ng, and R. Schober, "Joint beamforming and antenna movement design for moveable antenna systems based on statistical CSI," in *Proc. IEEE GLOBECOM*. IEEE, 2023, pp. 4387–4392.
- [13] Y. Ye, L. You, J. Wang, H. Xu, K.-K. Wong, and X. Gao, "Fluid antenna-assisted MIMO transmission exploiting statistical CSI," *IEEE Commun. Lett.*, Jan. 2024.
- [14] Z. Cheng, N. Li, J. Zhu, X. She, C. Ouyang, and P. Chen, "Enabling secure wireless communications via movable antennas," in *Proc. IEEE ICASSP*, Mar. 2024, pp. 9186–9190.
- [15] J. Tang, C. Pan, Y. Zhang, H. Ren, and K. Wang, "Secure MIMO communication relying on movable antennas," 2024, *arXiv: 2403.04269*. [Online]. Available: <https://arxiv.org/abs/2403.04269>
- [16] G. Hu, Q. Wu, K. Xu, J. Si, and N. Al-Dhahir, "Secure wireless communication via movable-antenna array," *IEEE Signal Process. Lett.*, vol. 31, pp. 516–520, Jan. 2024.
- [17] G. Hu, Q. Wu, D. Xu, K. Xu, J. Si, Y. Cai, and N. Al-Dhahir, "Movable antennas-assisted secure transmission without eavesdroppers' instantaneous CSI," 2024, *arXiv: 2404.03395*. [Online]. Available: <https://arxiv.org/abs/2404.03395>
- [18] L. Zhu, W. Ma, Z. Xiao, and R. Zhang, "Performance analysis and optimization for movable antenna aided wideband communications," 2024, *arXiv: 2401.08974*. [Online]. Available: <https://arxiv.org/abs/2401.08974>
- [19] L. Zhu, W. Ma, B. Ning, and R. Zhang, "Movable-antenna enhanced multiuser communication via antenna position optimization," *IEEE Trans. Wireless Commun.*, Dec. 2023, early access, doi: 10.1109/TWC.2023.3338626.
- [20] G. Hu, Q. Wu, K. Xu, J. Ouyang, J. Si, Y. Cai, and N. Al-Dhahir, "Movable-antenna array enabled multiuser uplink: A low-complexity gradient descent for total transmit power minimization," 2023, *arXiv: 2312.05763*. [Online]. Available: <https://arxiv.org/abs/2312.05763>
- [21] Z. Xiao, X. Pi, L. Zhu, X.-G. Xia, and R. Zhang, "Multiuser communications with movable-antenna base station: Joint antenna positioning, receive combining, and power control," 2023, *arXiv: 2308.09512*. [Online]. Available: <https://arxiv.org/abs/2308.09512>
- [22] Y. Sun, H. Xu, C. Ouyang, and H. Yang, "Sum-rate optimization for RIS-aided multiuser communications with movable antenna," 2023, *arXiv: 2311.06501*. [Online]. Available: <https://arxiv.org/abs/2311.06501>
- [23] G. Hu, Q. Wu, J. Ouyang, K. Xu, Y. Cai, and N. Al-Dhahir, "Movable-antenna array-enabled wireless communication with CoMP reception," 2023, *arXiv: 2311.11814*. [Online]. Available: <https://arxiv.org/abs/2311.11814>
- [24] Z. Cheng, N. Li, J. Zhu, X. She, C. Ouyang, and P. Chen, "Sum-rate maximization for fluid antenna enabled multiuser communications," *IEEE Commun. Lett.*, Mar. 2024, early access, doi: 10.1109/LCOMM.2024.3378272.
- [25] H. Qin, W. Chen, Z. Li, Q. Wu, N. Cheng, and F. Chen, "Antenna positioning and beamforming design for fluid antenna-assisted multi-user downlink communications," *IEEE Wireless Commun. Lett.*, Apr. 2024.
- [26] S. Yang, W. Lyu, B. Ning, Z. Zhang, and C. Yuen, "Flexible precoding for multi-user movable antenna communications," 2024, *arXiv: 2402.18847*. [Online]. Available: <https://arxiv.org/abs/2402.18847>
- [27] C. Weng, Y. Chen, L. Zhu, and Y. Wang, "Learning-based joint beamforming and antenna movement design for movable antenna systems," 2024, *arXiv: 2404.01784*. [Online]. Available: <https://arxiv.org/abs/2404.01784>
- [28] W. Mei, X. Wei, B. Ning, Z. Chen, and R. Zhang, "Movable-antenna position optimization: A graph-based approach," 2024, *arXiv: 2403.16886*. [Online]. Available: <https://arxiv.org/abs/2403.16886>
- [29] Y. Zhang, Y. Zhang, L. Zhu, S. Xiao, W. Tang, Y. C. Eldar, and R. Zhang, "Movable antenna-aided hybrid beamforming for multi-user communications," 2024, *arXiv: 2404.00953*. [Online]. Available: <https://arxiv.org/abs/2404.00953>
- [30] Y. Wu, D. Xu, D. W. K. Ng, W. Gerstacker, and R. Schober, "Movable antenna-enhanced multiuser communication: Jointly optimal discrete antenna positioning and beamforming," in *Proc. IEEE GLOBECOM*. IEEE, Dec. 2023, pp. 7508–7513.
- [31] B. Lyu, H. Liu, W. Hong, S. Gong, and F. Tian, "Primary rate maximization in movable antennas empowered symbiotic radio communications," 2023, *arXiv: 2403.14943*. [Online]. Available: <https://arxiv.org/abs/2403.14943>
- [32] J. Ding, Z. Zhou, C. Wang, W. Li, L. Lin, and B. Jiao, "Secure full-duplex communication via movable antennas," 2023, *arXiv: 2403.20025*. [Online]. Available: <https://arxiv.org/abs/2403.20025>
- [33] H. Wang, Q. Wu, and W. Chen, "Movable antenna enabled interference network: Joint antenna position and beamforming design," 2024, *arXiv: 2403.13573*. [Online]. Available: <https://arxiv.org/abs/2403.13573>
- [34] W. Ma, L. Zhu, and R. Zhang, "Compressed sensing based channel estimation for movable antenna communications," *IEEE Commun. Lett.*, Oct. 2023.
- [35] Z. Xiao, S. Cao, L. Zhu, Y. Liu, X.-G. Xia, and R. Zhang, "Channel estimation for movable antenna communication systems: A framework based on compressed sensing," 2023, *arXiv: 2312.06969*. [Online]. Available: <https://arxiv.org/abs/2312.06969>
- [36] Z. Zhang, J. Zhu, L. Dai, and R. W. Heath Jr, "Successive bayesian reconstructor for channel estimation in flexible antenna systems," 2023, *arXiv: 2312.06551*. [Online]. Available: <https://arxiv.org/abs/2312.06551>
- [37] S. Boyd and L. Vandenberghe, *Convex Optimization*. Cambridge, U.K.: Cambridge Univ. Press, 2004.
- [38] Y. Sun, P. Babu, and D. P. Palomar, "Majorization-minimization algorithms in signal processing, communications, and machine learning," *IEEE Trans. Signal Process.*, vol. 65, no. 3, pp. 794–816, Feb. 2017.
- [39] Q. Wu, Y. Zeng, and R. Zhang, "Joint trajectory and communication design for multi-UAV enabled wireless networks," *IEEE Trans. Wireless Commun.*, vol. 17, no. 3, pp. 2109–2121, Mar. 2018.
- [40] K. Wang, A. M. So, T. Chang *et al.*, "Outage constrained robust transmit optimization for multiuser MISO downlinks: Tractable approximations by conic optimization," *IEEE Trans. Signal Process.*, vol. 62, no. 21, pp. 5690–5705, Nov. 2014.
- [41] H. Joudeh and B. Clerckx, "Rate-splitting for max-min fair multigroup multicast beamforming in overloaded systems," *IEEE Trans. Wireless Commun.*, vol. 16, no. 11, pp. 7276–7289, Nov. 2017.